RELATIVE PERIODIC SOLUTIONS OF THE COMPLEX GINZBURG-LANDAU EQUATION *

VANESSA LÓPEZ†¶, PHILIP BOYLAND‡, MICHAEL T. HEATH†, AND ROBERT D. MOSER§

Abstract. A method of finding relative periodic orbits for differential equations with continuous symmetries is described and its utility demonstrated by computing relative periodic solutions for the one-dimensional complex Ginzburg-Landau equation (CGLE) with periodic boundary conditions. A relative periodic solution is a solution that is periodic in time, up to a transformation by an element of the equation's symmetry group. With the method used, relative periodic solutions are represented by a space-time Fourier series modified to include the symmetry group element and are sought as solutions to a system of nonlinear algebraic equations for the Fourier coefficients, group element, and time period. The 77 relative periodic solutions found for the CGLE exhibit a wide variety of temporal dynamics, with the sum of their positive Lyapunov exponents varying from 5.19 to 60.35 and their unstable dimensions from 3 to 8. Preliminary work indicates that weighted averages over the collection of relative periodic solutions accurately approximate the value of several functionals on typical trajectories.

Key words. Relative periodic solutions, Ginzburg-Landau equation, Spectral-Galerkin method, Chaotic pattern dynamics

AMS subject classifications. 35B10, 65N35, 65N22

1. Introduction. The complex Ginzburg-Landau equation (CGLE) is a widely studied partial differential equation with applications in many areas of science. (See [1, 44] and references therein.) It has become a model problem for the study of nonlinear evolution equations with chaotic spatio-temporal dynamics. In this paper we work with the CGLE with cubic nonlinearity in one spatial dimension,

$$\frac{\partial A}{\partial t} = RA + (1 + \mathrm{i}\nu)\frac{\partial^2 A}{\partial x^2} - (1 + \mathrm{i}\mu)A|A|^2, \tag{1.1}$$

with periodic boundary conditions

$$A(x,t) = A(x + 2\pi, t), \tag{1.2}$$

and, as a convention, when we refer to *the CGLE* we mean equation (1.1) with the boundary conditions (1.2), unless otherwise noted. Equation (1.1) describes the evolution of a complex-valued field $A(x,t)$. The parameters R, ν, and μ are real. When $R < 0$ all solutions converge to $A = 0$ in forward time, but when $R > 0$

*This work was partially supported by NSF Grant CTS 97-29189 and by the endowment for the Fulton Watson Copp Chair in Computer Science at the University of Illinois.

†Department of Computer Science, University of Illinois, Urbana, IL, USA (vlopez@cse.uiuc.edu, heath@cs.uiuc.edu).

‡Mathematics Department, University of Florida, Gainesville, FL, USA (boyland@math.ufl.edu).

§Department of Theoretical and Applied Mechanics, University of Illinois, Urbana, IL, USA. Current address: Mechanical Engineering Department, The University of Texas at Austin, 1 University Station C2200, Austin, TX, USA (rmoser@mail.utexas.edu).

¶Corresponding author. Current address: Lawrence Berkeley National Lab, 1 Cyclotron Road, Mail Stop 50F1650, Berkeley, CA 94720, USA. E-mail: vlopez@hpcrd.lbl.gov.

there is, in general, nontrivial spatio-temporal behavior. The parameters ν and μ are measures of the linear and nonlinear dissipation, respectively. (See, for example, [1, 22, 39, 59] for further details.) It is known that in the form (1.1) the CGLE generates a continuous semiflow on a variety of spaces [5, 21, 39, 56].

The CGLE has a three-parameter group $\mathbb{T}^2 \times \mathbb{R}$ of continuous symmetries generated by space-time translations and a rotation of the complex field A. That is, if $A(x,t)$ is a solution of the CGLE, then so is $\mathrm{e}^{\mathrm{i}\eta_1} A(x+\eta_2, t+\tau)$ for any element (η_1, η_2) of the two-torus $\mathbb{T}^2$ and $\tau \in \mathbb{R}$. Thus, we focus our study on time-periodic solutions of the CGLE relative to the $\mathbb{T}^2$-symmetry, namely, solutions of the CGLE that satisfy

$$A(x,t) = \mathrm{e}^{\mathrm{i}\varphi} A(x+S, t+T) \tag{1.3}$$

for some $(\varphi, S) \in \mathbb{T}^2$ and $T > 0$. Note that after a period of time T, such a solution returns not to itself, but rather to an element in its $\mathbb{T}^2$-orbit. Such *relative periodic solutions* represent invariant three-tori in the CGLE flow. Previous studies of time-periodic solutions of the CGLE (1.1) have centered on two types of solutions. The first are single-frequency solutions of the form $A(x,t) = B(x)\mathrm{e}^{\mathrm{i}\omega t}$ (see, for example, [15, 20, 30]); these are referred to as *stationary solutions*. The second type are generalized traveling waves, also called *coherent structures*, for which $A(x,t) = \rho(x-vt)\mathrm{e}^{\mathrm{i}\phi(x-vt)}\mathrm{e}^{\mathrm{i}\omega t}$, where ρ and ϕ are real-valued functions and ω is some frequency (see, for example, [1, 7, 44, 58]). These coherent structures reduce to single-frequency solutions by a change to a moving frame, that is, by a change of variables $x \to x + vt$, $t \to t$. The relative periodic solutions of interest in this study are different in that they exhibit more complicated temporal behavior than the single-frequency solutions just described. Studies of bifurcations to (stable) invariant two and three-tori for the CGLE are described in [55] and references therein. The relative periodic solutions we compute, which represent invariant three-tori, are obtained by working with fixed parameter values for the CGLE, as described below (and in more detail in § 3.4 and § 4), not via a bifurcation study.

We employ a spectral-Galerkin procedure to compute relative periodic solutions of the CGLE. A solution to equation (1.3) is constructed and is then used to represent the relative periodic solutions. This ansatz consists of a Fourier series in both space and time, modified to include the $\mathbb{T}^2$ element (φ, S) as an unknown. Substitution of the ansatz into the differential equation yields a system of nonlinear algebraic equations, the solutions of which give the desired relative periodic solutions. Using this procedure we were able to identify 77 distinct relative periodic solutions of the CGLE with parameters $R = 16$, $\nu = -7$, and $\mu = 5$. These parameter values were chosen because for them the system exhibits temporal chaos, yet the value of R is such that a relatively small number of spatial modes can capture the dynamics of the system.

The task of computing relative periodic solutions was undertaken as a first step in understanding the dynamics of the CGLE with the chosen parameters. The 77 relative periodic solutions are neither stationary nor coherent structures (as defined earlier), but two stationary solutions were also found. Aside from these two single-frequency solutions, we found no (truly) time-periodic solutions. For each relative periodic solution, the largest Lyapunov exponent ranges from 1.88 to 17.20, the sum of the positive Lyapunov exponents from 5.19 to 60.35, and the unstable dimension from 3 to 8. In particular, the system displays unstable dimension variability, a phenomenon that a number of recent papers have indicated is central to the understanding of high-dimensional dynamical systems; see, for example, [33, 54].

In a general context, the study of periodic orbits has been a basic tool in the theory of dynamical systems for at least 100 years. Typically, there are infinitely many different periodic solutions embedded in a chaotic attractor. Using tools from periodic orbit theory, statistical averages that provide a description of the asymptotic behavior of a chaotic dynamical system can be approximated from the short-term dynamics of the (unstable) periodic solutions on an attractor of the chaotic system [13, 14]. Periodic solutions of chaotic dynamical systems are also used in techniques for controlling chaos. Given a set of unstable periodic solutions of a chaotic dynamical system, the chaos could be mitigated by applying small, time-dependent perturbations to stabilize trajectories onto chosen periodic solutions. This is the basis of the Ott-Grebogi-Yorke approach for controlling chaos; see, for example, [50].

(True) periodic solutions of dynamical systems have been computed with a variety of methods. The use of Fourier series along with the numerical solution of systems of nonlinear algebraic equations is common (as in [37, 40, 57]), but the use of multiple shooting algorithms for boundary value problems, which combine numerical integration and the solution of systems of nonlinear algebraic equations, is also popular (see, for example, [10, 13, 28]). Furthermore, expansions other than Fourier series, for example, Taylor series expansions [28] and piecewise polynomials [19], are also utilized. More recently, a variational method for finding (true) periodic solutions was proposed [36].

Often, the suitability of a numerical method for computing periodic solutions is illustrated by applying the method to low-dimensional dynamical systems (2–4 equations). Higher dimensional systems have been considered in [11], [36], and [62] (with 16, 32, and 99 equations, respectively), where (true) periodic solutions of the Kuramoto-Sivashinsky equation were computed. The system studied in [11] has a low-dimensional chaotic attractor; those in [62] and [36] have higher intrinsic dimension. In particular, the system considered in [62] has a Lyapunov dimension of 8.8 [41], with typical trajectories having four positive and one zero Lyapunov exponent. We also work with a high-dimensional system (62 real ordinary differential equations) when computing relative periodic solutions of the CGLE. The system we study has a Lyapunov dimension of approximately 11.52; typical trajectories in our system have five positive and three zero Lyapunov exponents.

2. Symmetries and Differential Equations. In this section we review some standard definitions and results concerning differential equations with continuous symmetries. For more information see, for example, [27, 43, 45, 49]. Properties of relative equilibria and relative periodic orbits are given in [23, 24, 34, 35, 60, 61].

2.1. Basic Definitions. Under suitable hypotheses, a vector field $\mathbf{X}$, a differential equation

$$\dot{z} = \mathbf{X}(z) \tag{2.1}$$

on a space B, and an $\mathbb{R}$-action or flow $\phi : \mathbb{R} \times B \to B$ are connected by

$$\mathbf{X}(\phi_t(z)) = \frac{\partial \phi_t(z)}{\partial t},$$

where $\phi_t(z)$ is commonly used for $\phi(t, z)$. The *trajectory* of a flow with initial condition z_0 is $\{\phi_t(z_0) : t \in \mathbb{R}\}$ and is also called a *flow orbit* or a *solution*. A curve $\gamma(t)$ is said to be a solution of (2.1) if $\gamma(t) = \phi_t(z_0)$ for some $z_0 \in B$.

Continuous symmetries are expressed by the smooth left action of a Lie group G on B, where we write $g \cdot z$ for the action of the element $g \in G$ on $z \in B$. For

simplicity of exposition we assume that G is compact and connected and acts linearly on the linear space B. The differential equation (2.1) is said to be *equivariant under the group action* if $g \cdot \mathbf{X}(z) = \mathbf{X}(g \cdot z)$ for all $g \in G$ and $z \in B$. If ϕ_t is the flow of $\mathbf{X}$, then G-equivariance of $\mathbf{X}$ is equivalent to

$$g \cdot \phi_t(z) = \phi_t(g \cdot z) \tag{2.2}$$

for all g, z, and t, and one also speaks of the flow being G-equivariant. Since the vector field $\mathbf{X}$ is assumed to be time-independent, the equation (2.1) is invariant under the product action of $G \times \mathbb{R}$ given by $(g, \tau) \cdot z(t) = g \cdot z(t + \tau)$.

The *group orbit* of $z \in B$ under the G-action is $G \cdot z = \{g \cdot z : g \in G\}$. If the group acting is clear from the context, this orbit will also be denoted by $\mathcal{O}_z$. The *isotropy subgroup or stabilizer* of z is $G_z = \{g \in G : g \cdot z = z\}$, and the group orbit $G \cdot z$ is diffeomorphic to the quotient G/G_z. As a consequence of (2.2), the stabilizer is constant on a trajectory, that is, $G_{\phi_t(z)} = G_z$ for all t, so one may speak unambiguously of the G-stabilizer of a flow trajectory or of the topological type of its G-orbit. In addition, if $H \subset G$ is a subgroup, then its fixed subspace $\mathrm{Fix}(H) = \{z \in B : h \cdot z = z \text{ for all } h \in H\}$ is flow invariant.

2.2. Relative Equilibria and Relative Periodic Orbits. There are two equivalent points of view from which one can discuss the influence of symmetries on the dynamics of (2.1). The first is to consider the family of trajectories that arise by applying symmetry operations to a given trajectory. The second is to note that (2.2) implies that the flow on B descends to a flow on the quotient space B/G, and then study the dynamics of this *reduced flow*.

To pursue the first point of view, note that (2.2) implies that given the trajectory with initial condition z_0, the trajectory with initial condition $g \cdot z_0$ can be obtained by applying the symmetry g to the trajectory of z_0. Thus, the equivariance of the flow implies that trajectories come in families related by the symmetries. For a given z_0, the union of all the members of this family is equal to the group orbit of z_0 under the joint action of $\Gamma := (G \times \mathbb{R})$ on B given by $(g, \tau) \cdot z = \phi_\tau(g \cdot z) = g \cdot \phi_\tau(z)$. Thus, each initial condition generates a flow invariant set $\Gamma \cdot z_0$, and we may consider these Γ-orbits as the principal dynamical objects associated with the differential equation with symmetry.

The simplest case of a Γ-orbit occurs when z_0 projects to a rest point of the reduced flow. This occurs exactly when the G-orbit of z_0 is flow invariant, and so the Γ-orbit of z_0 is equal to its G-orbit. In this case the set $\Gamma \cdot z_0$ is called a *relative equilibrium*, and the point z_0 is said to be an element of the relative equilibrium. When z_0 is an element of a relative equilibrium, its flow trajectory is always equal to the action on z_0 of a one-parameter subgroup $\sigma(t)$ of G, that is,

$$\phi_t(z_0) = \sigma(t) \cdot z_0. \tag{2.3}$$

The case of primary interest here are Γ-orbits that project to periodic orbits of the reduced flow. The sets are called *relative periodic orbits*. Thus, a point z_0 is an element of a relative periodic orbit if and only if

$$z_0 = g_0 \cdot \phi_T(z_0) \tag{2.4}$$

for some $g_0 \in G$ and $T > 0$. Since a relative equilibrium in the form (2.3) will satisfy (2.4) for $g_0 = \sigma(t)$ and $T = t$, for any t, we explicitly include in the definition the requirement that a relative periodic orbit is *not* a relative equilibrium. The group

element g_0 is called the *drift*, and T is the *period*. If z_0 is an element of a relative periodic orbit, then its Γ-orbit is diffeomorphic to $(G \cdot z_0) \times S^1$. We will refer to the flow orbit of a point z_0 satisfying (2.4) as a (g_0, T)-*relative periodic orbit or solution*, and when it is clear from the context (in a slight abuse of terminology), simply as a relative periodic orbit or solution.

Note that if (2.4) holds, then $\phi_t(z_0) = g_0 \cdot \phi_{t+T}(z_0)$ for all t. Also note that (2.4) does not uniquely determine g_0 and T: a (g_0, T)-relative periodic orbit is also a (g_0^k, kT)-relative periodic orbit for any integer k, as well as a $(g_0 g', T)$-relative periodic orbit for any $g' \in G_{z_0}$. However, if z_0 is an element of a relative periodic orbit, then there is a least positive T for which $\phi_t(z_0)$ is a (g_0, T)-relative periodic orbit for some $g_0 \in G$. Thus, we adopt the convention that when a relative periodic orbit is said to have drift and period (g_0, T) the period is always this least positive T. Even with this convention, the drift g_0 is still defined only up to the stabilizer G_{z_0}.

Finally, we remark that there is a variety of terminology used in the literature for relative periodic orbits and relative equilibria. In particular, the meaning of the term "drift" is not completely uniform, and in Hamiltonian dynamics what is called the drift here is called, depending on the context, a reconstruction, geometric, or other variety of phase. Also note that the definitions and results of this section extend easily to semiflows with continuous symmetries.

3. CGLE: Symmetries and Temporal Dynamics. The CGLE in the form (1.1) with periodic boundary conditions generates a continuous semiflow on $\mathcal{S} := L^2(S^1)$ as well as on other spaces requiring greater regularity [5, 21, 39, 56]. The semiflow on $\mathcal{S}$ is known to have a finite dimensional attracting set or universal attractor as well as a Lipschitz inertial manifold [5, 12, 22, 26, 53]. Further, on the universal attractor the CGLE generates a flow (i.e., solutions that are bounded and defined for all time), and elements of the attractor are in fact C^ω-functions [21].

3.1. Symmetries and Associated ODEs. The CGLE has a number of well known symmetries that are central to its behavior and our study (see, for example, [3, 4]). If $A(x,t)$ is a solution of (1.1), then so are

$$\mathrm{e}^{\mathrm{i}\eta_1} A(x,t), \tag{3.1}$$

$$A(x+\eta_2, t), \tag{3.2}$$

$$A(x, t+\tau), \tag{3.3}$$

$$A(-x, t), \tag{3.4}$$

where η_1, η_2, and τ are any real numbers. Since the η_i can be treated mod 2π, (3.1) and (3.2) say that the CGLE semiflow is equivariant under the action of the two-torus group $\mathbb{T}^2$ on $\mathcal{S}$ with the action on $\alpha \in \mathcal{S}$ given by $(\eta_1, \eta_2) \cdot \alpha(x) = \mathrm{e}^{\mathrm{i}\eta_1} \alpha(x + \eta_2)$. The symmetry (3.3) corresponds to translation along the semiflow. The $\mathbb{Z}_2$-action expressed by (3.4) will be important in describing properties of specific solutions in § 5.2, but in most of this paper the continuous symmetries will be our primary concern.

Since the chosen boundary conditions for the CGLE (1.1) are periodic in x, we may use spatial Fourier series to transform into $\mathcal{C} := \ell_b^2(\mathbb{C})$, the space of all square-summable bi-infinite, complex sequences. Thus, we write

$$A(x,t) = \sum_{m \in \mathbb{Z}} a_m(t) \mathrm{e}^{\mathrm{i}mx}, \tag{3.5}$$

substitute into (1.1), and obtain an infinite system of ODEs,

$$\frac{\mathrm{d}a_m}{\mathrm{d}t} = Ra_m - m^2(1+\mathrm{i}\nu)a_m - (1+\mathrm{i}\mu)\sum_{m_1+m_2-m_3=m} a_{m_1}a_{m_2}a^*_{m_3}, \tag{3.6}$$

for the complex-valued functions $a_m(t)$.

Under this transformation the symmetries of (1.1) become symmetries of (3.6). Thus, if $(a_m(t))$ is a solution of (3.6), then so are

$$(\mathrm{e}^{\mathrm{i}\eta_1}a_m(t)), \tag{3.7}$$

$$(\mathrm{e}^{\mathrm{i}m\eta_2}a_m(t)), \tag{3.8}$$

$$(a_m(t+\tau)), \tag{3.9}$$

$$(a_{-m}(t)). \tag{3.10}$$

In particular, (3.7) and (3.8) say that the ODEs (3.6) are invariant under an action of $\mathbb{T}^2$ on $\mathcal{C}$, with the action on $\boldsymbol{a} = (a_m) \in \mathcal{C}$ given by

$$(\eta_1, \eta_2) \cdot (a_m) = (\mathrm{e}^{\mathrm{i}\eta_1}\mathrm{e}^{\mathrm{i}m\eta_2}a_m). \tag{3.11}$$

In all our computations with the CGLE we work with the spectral Galerkin projection obtained by fixing an even number N_x, truncating the expansion (3.5) to include the indices m with $-N_x/2+1 \le m \le N_x/2-1$, and considering only the corresponding ODEs from (3.6). Much accumulated theory and computation demonstrates that for sufficiently large N_x the behavior of this truncation captures the essential features of the dynamics of (1.1) [21, 29].

The system of N_x-1 complex ODEs resulting from the Galerkin projection has the same symmetries as the infinite system. The $\mathbb{T}^2$-action is linear on the finite-dimensional space $\mathbb{C}^{N_x-1}$, with a group element $(\eta_1, \eta_2) \in \mathbb{T}^2$ acting via multiplication by the unitary matrix $\mathrm{diag}(\mathrm{e}^{\mathrm{i}\eta_1}\mathrm{e}^{\mathrm{i}m\eta_2})$, where it is understood that the indexing is by increasing value of m, that is, $m = -N_x/2+1, \ldots, N_x/2-1$. Henceforth this ordering is assumed whenever applicable. For convenience, we denote the truncated system of ODEs as

$$\frac{\mathrm{d}\boldsymbol{a}}{\mathrm{d}t} = \mathbf{X}(\boldsymbol{a}). \tag{3.12}$$

3.2. Stabilizers, Group Orbits, and Invariant Subspaces. For our discussion of the temporal dynamics and relative periodic solutions of the CGLE it will be useful to have a catalog of the various stabilizers, group orbits and fixed subspaces. These facts are well known and elementary. It is simplest to work with the $\mathbb{T}^2$-action on $\mathcal{C}$ given by (3.11) and then transfer the conclusions to $\mathcal{S}$.

The only point in $\mathcal{C}$ fixed by all of $\mathbb{T}^2$ is $\boldsymbol{a} = \mathbf{0}$, so henceforth we only consider nonzero elements and proper subgroups of $\mathbb{T}^2$. The nontrivial isotropy subgroups are of two classes. The first class consists of finite cyclic subgroups of $\mathbb{T}^2$ generated by elements of the form $(2\pi k/q, 2\pi/q)$, for integers q and k with $0 < q$ and $0 \le k < q$. Note that k and q may have common factors. These groups will be denoted $C(k,q)$. The fixed subspaces corresponding to these cyclic subgroups are $\mathrm{Fix}(C(k,q)) = \{(a_m) : a_m = 0 \text{ if } m \neq -k \mod q\}$, and the stabilizer of (a_m) is $C(k,q)$ exactly when $(a_m) \in \mathrm{Fix}(C(k,q))$ and the least $m > 0$ with $a_m \neq 0$ is $m = q-k$. The points with this stabilizer have group orbits diffeomorphic to a two-torus and correspond to $\alpha \in \mathcal{S}$ which satisfy $\alpha(x) = \mathrm{e}^{\mathrm{i}2\pi k/q}\alpha(x+2\pi/q)$.

The second class of stabilizers consists of one-dimensional subgroups of $\mathbb{T}^2$ of the form $\{(pu, u) : u \in S^1\}$ for integers p. These groups will be denoted $D(p)$. The fixed subspaces corresponding to these one-dimensional subgroups are $\mathrm{Fix}(D(p)) = \{(a_m) : a_m = 0 \text{ if } m \neq p\}$, and the stabilizer of (a_m) is $D(p)$ exactly when $(a_m) \in \mathrm{Fix}(D(p))$. The points with this stabilizer have group orbits diffeomorphic to the circle and correspond to $\alpha \in \mathcal{S}$ of the form $\alpha(x) = a_p e^{ipx}$ for a fixed nonzero $a_p \in \mathbb{C}$.

Now recall that each subspace fixed by a subgroup of $\mathbb{T}^2$ is invariant under the CGLE semiflow. Using the ODEs (3.6), the semiflow restricted to each $\mathrm{Fix}(D(p))$ is easily understood. If $p^2 \geq R$, then all trajectories in $\mathrm{Fix}(D(p))$ converge to zero in forward time. If $p^2 < R$, then all trajectories in $\mathrm{Fix}(D(p))$ are attracted to what is usually called the *plane wave*,

$$A(x,t) = ce^{i\omega t}e^{ipx}, \tag{3.13}$$

for $R = p^2 + c^2$ and $\omega = -\nu p^2 - \mu c^2$.

The dynamics on the subspaces $\mathrm{Fix}(C(k,q))$ are in general quite complicated. But it is worth noting that the transformation $A(x,t) = q^2 B(qx, q^2 t)$ is a bijection between solutions $A(x,t)$ of (1.1) with isotropy subgroup $C(0,q)$ and solutions B of (1.1) with the same ν and μ but with the R coefficient equal to R/q^2. Thus, all the relative periodic solutions for $R = 16$ described in § 5 are present, after a change of coordinates, in invariant subspaces for $R = 16n^2$, for all integers n.

Finally, since the focus here is on relative periodic solutions with respect to the $\mathbb{T}^2$-symmetry, we mention only briefly the $\mathbb{Z}_2$-symmetry acting as in (3.4) or (3.10). The new class of fixed subspaces consist of elements of $\mathcal{S}$ that satisfy

$$\alpha(-x + \eta_2) = \alpha(x) \quad \text{or} \quad -\alpha(-x + \eta_2) = \alpha(x), \tag{3.14}$$

that is, they are even or odd with respect to reflection about $\eta_2/2$.

3.3. Relative Equilibria and Relative Periodic Solutions. One-parameter subgroups of $\mathbb{T}^2$ can be written as $(\omega_1 t, \omega_2 t)$, so the relative equilibria of the CGLE (1.1) contain solutions of the form

$$A(x,t) = e^{i\omega_1 t}\alpha(x + \omega_2 t)$$

for $\alpha \in \mathcal{S}$. When $\omega_2 = 0$, these solutions have a single temporal frequency and are called *steady solutions*. When $\omega_1 = 0$, the solution is a traveling wave, and when both group elements are nonzero the solution is what is called a *generalized traveling wave* or *coherent structure*. These have been extensively studied in the literature (see, for example, [1, 44, 58]).

A relative periodic orbit of the CGLE with drift (φ, S) and period T contains solutions that satisfy $A(x,t) = e^{i\varphi}A(x+S, t+T)$ for all t. The corresponding solution of the system of ODEs (3.6) thus satisfies

$$a_m(t) = e^{i\varphi}e^{imS}a_m(t+T) \tag{3.15}$$

for all m and t. Note that the only recurrent trajectories with stabilizers $D(p)$ are the plane waves (3.13), which are relative equilibria. Since by definition a relative periodic orbit is not a relative equilibrium, any relative periodic orbit of the CGLE has a $\mathbb{T}^2$-stabilizer that is either trivial or finite, and thus its group orbit is a two-torus. Thus, a relative periodic orbit of the CGLE is diffeomorphic to a three-torus, so each solution described in § 5 yields an invariant three-torus in the CGLE semiflow.

By virtue of (3.4), if $A(x,t)$ is a solution of the CGLE, then so is $A(-x,t)$. This implies that a relative periodic solution typically yields two distinct invariant three-tori in the CGLE semiflow. However, if the solution possesses the symmetry (3.14), these tori are identified.

We finally remark that the task of finding a relative equilibrium for the CGLE can be reduced to solving a three-dimensional system of ordinary differential equations with parameters (see, for example, [1]). No such simplification appears to be possible for finding relative periodic solutions of the CGLE.

3.4. Dynamics for Selected Parameter Values. The parameter values $R = 16$, $\nu = -7$, and $\mu = 5$ were selected for our study. For these parameter values the numerical computation of the largest Lyapunov exponent λ_1 of 50 typical trajectories evolved from time $t = 0$ to $t = 600$ gave a mean value of $\lambda_1 \approx 5.36$, with a standard deviation of 0.11. We obtained a value of approximately 11.52 for the Lyapunov (or Kaplan-Yorke) dimension, with a standard deviation of 0.04. As a consequence of the $\mathbb{T}^2$-symmetry, each trajectory has two Lyapunov exponents equal to zero [2], in addition to the zero exponent in the flow direction. These three exponents were included in calculation of the Lyapunov dimension. A typical trajectory has five positive Lyapunov exponents, and thus an unstable manifold with real dimension 5. The sum of the positive Lyapunov exponents (which will henceforth be called the *total instability*) was typically equal to approximately 15.71, with a standard deviation of 0.40.

The fairly small deviations from the mean for these dynamical quantities justify referring to them as "typical values", but we use this term without any claim of the existence of any particular class of ergodic invariant measure. Similarly, we will speak of the typical trajectories as being contained in a main attractor without claiming that it is indecomposable in any sense. If we accept the Kaplan-Yorke and related conjectures, then the computed Lyapunov dimension indicates that the main attractor has fractal dimension equal to 11.52. The terminology "main attractor" refers to the closure of the typical trajectories and is distinguished from the "universal attractor" whose existence is proved in [5, 12, 22, 26]. The latter, which would be called a global attracting set in topological dynamics, refers to the intersection of the forward images of a forward invariant set that is globally attracting. In particular, the universal attractor can contain trajectories that are not typical in the sense just described. For example, the Lyapunov spectra of the rest point $\mathbf{0}$ and the plane waves, as reported in Appendix A, Table A.2, are very different from those of typical trajectories and from those of the relative periodic solutions reported in Table A.1.

When comparing the results here with those in the literature it is important to note that in addition to (1.1) there are other forms of the CGLE that appear in the literature. The most common alternative is to fix the coefficient of A as 1,

$$\frac{\partial \tilde{A}}{\partial t} = \tilde{A} + (1 + \mathrm{i}\nu)\frac{\partial^2 \tilde{A}}{\partial x^2} - (1 + \mathrm{i}\mu)\tilde{A}|\tilde{A}|^2, \tag{3.16}$$

and have periodic boundary conditions, $\tilde{A}(x + L, t) = \tilde{A}(x, t)$. The transformation

$$A(x,t) = \sqrt{R}\,\tilde{A}(\sqrt{R}\,x, R\,t) \tag{3.17}$$

takes a solution A of (1.1) to a solution $\tilde{A}$ of (3.16) with period $L = 2\pi\sqrt{R}$ in x. In particular, the parameter value of $R = 16$ used here corresponds to solving (3.16) with $L = 8\pi \approx 25.13$ and the commonly used value of $L = 512$ in (3.16) corresponds to

$R \approx 6640$ in (1.1). The range of periods $0.02 < T < 0.46$ described in § 5 corresponds to periods $0.32 < T < 7.36$ for (3.16). Note also that the rescaling of time in (3.17) rescales Lyapunov exponents and so will alter the total instability of a trajectory but not its Lyapunov dimension or its unstable dimension.

The value $R = 16$ used in this paper for the CGLE in the form (1.1) is comparable to that of other studies of the CGLE temporal dynamics (for example, [32, 46]), but is much less than the corresponding R value used in most studies of the spatiotemporal behavior of the CGLE. The parameters as chosen have the advantage that the temporal dynamics are chaotic and indeed, have a much higher intrinsic dimension than is usual in dynamical studies, but R is sufficiently small that a relatively small number of spatial Fourier modes suffices to capture the dynamics. As has been noted (for example in [9]), the dynamics of the CGLE at small R (or L) is quite different from that at larger values. As for the commonly used characterizations in terms of phase and defect turbulence, we note that for a typical trajectory of the CGLE at the chosen parameter values the modulus $|A(x,t)|$ frequently vanishes (defects) and the average phase gradient (i.e., the winding number about the origin of the image of $x \mapsto A(x,t)$ in the complex plane as shown, for example, in Figure 5.3) varies somewhat irregularly from -2 to 2. The chosen values of $\nu = -7$ and $\mu = 5$ are in the Benjamin-Feir unstable region $1 + \mu\nu < 0$, and the plane waves are unstable to sideband perturbations and have unstable dimension of 8 (see Appendix A, Table A.2).

4. Computing Relative Periodic Solutions. We now describe the procedure used to compute relative periodic solutions of the system of ODEs (3.12) and, thus, of the CGLE. Although the discussion is specifically for the problem of computing relative periodic solutions for the CGLE, the procedure is applicable to the general problem of computing relative periodic solutions of evolution equations with continuous symmetries.

4.1. From ODEs to Nonlinear Algebraic Equations. In seeking relative periodic solutions $\boldsymbol{a}(t)$ of the system of ODEs (3.12), we use the ansatz

$$a_m(t) = \mathrm{e}^{-\mathrm{i}\frac{\varphi}{T}t}\mathrm{e}^{-\mathrm{i}m\frac{S}{T}t}\sum_n \hat{a}_{m,n}\mathrm{e}^{\mathrm{i}n\frac{2\pi}{T}t} \tag{4.1}$$

and work with the Galerkin projection obtained by fixing an even number N_t, so that the summation index in (4.1) runs over the range $-N_t/2 + 1 \le n \le N_t/2 - 1$. The $a_m(t)$ given by (4.1) solve the equations (3.15) and hence are an appropriate representation for a relative periodic solution of the system of ODEs. Note that a (g,T)-relative periodic solution of the system of ODEs is in fact being represented as

$$\boldsymbol{a}(t) = \mathrm{e}^{-tL_g/T}\boldsymbol{b}(t/T), \tag{4.2}$$

where $g = (\varphi, S)$, L_g is the matrix $\mathrm{diag}(\mathrm{i}\varphi + \mathrm{i}mS)$, and $\boldsymbol{b}$ is periodic with period one. Since the action of $\mathbb{T}^2$ is linear on the space $\mathbb{C}^{N_x-1}$, substituting (4.2) into the system of ODEs (3.12) and using the $\mathbb{T}^2$-equivariance of $\mathbf{X}$ yields a system of equations for $\boldsymbol{b}$ and (g,T),

$$\frac{1}{T}\left(\frac{\mathrm{d}\boldsymbol{b}}{\mathrm{d}t} - L_g\boldsymbol{b}\right) = \mathbf{X}(\boldsymbol{b}),$$

from which one computes relative periodic solutions. We point out that (4.2) can be viewed as the passage into a moving frame in which the relative periodic solution is in

fact periodic. The moving frame is constructed using the appropriate one-parameter subgroup as in [60].

Indeed, in the general case of finding relative periodic orbits of a G-equivariant ODE, $\dot{z} = \mathbf{X}(z)$, one adopts the ansatz $z(t) = \mathrm{e}^{-\xi t/T} \cdot \beta(t/T)$, where ξ is in the Lie algebra of G and $\beta(t+1) = \beta(t)$. Substitution into the ODE and some manipulation yields that $z(t)$ is an (e^{ξ}, T)-relative periodic orbit if it satisfies

$$\frac{1}{T}\left(\frac{\mathrm{d}\beta}{\mathrm{d}t} - \mathbf{Y}_{\xi} \circ \beta\right) = \mathbf{X} \circ \beta, \tag{4.3}$$

where $\mathbf{Y}_{\xi}$ is the infinitesimal generator corresponding to ξ. The terms in (4.3) represent vector fields along the closed curve β with $\mathbf{Y}_{\xi} \circ \beta$ corresponding to the velocity vector induced by passage into the moving frame.

To be concrete, substituting (4.1) into the truncated system of ODEs (3.6) results in a system of nonlinear algebraic equations,

$$\begin{aligned} \mathrm{i}\left(\frac{2\pi n}{T} - \frac{\varphi}{T} - m\frac{S}{T}\right)\hat{a}_{m,n} \;&=\; R\hat{a}_{m,n} - m^2(1+\mathrm{i}\nu)\hat{a}_{m,n} \\ &\quad - (1+\mathrm{i}\mu)\sum_{m_1+m_2-m_3=m}\left(\sum_{n_1+n_2-n_3=n}\hat{a}_{m_1,n_1}\hat{a}_{m_2,n_2}\hat{a}^*_{m_3,n_3}\right), \end{aligned} \tag{4.4}$$

for the complex Fourier coefficients $\{\hat{a}_{m,n}\}$, the drift (φ, S), and the time period T. Therefore, (4.4) is an underdetermined system of $(N_x-1)(N_t-1)$ complex equations in $(N_x-1)(N_t-1)$ complex unknowns plus three real unknowns or, after splitting the equations into their real and imaginary parts, $2(N_x-1)(N_t-1)$ real equations in $2(N_x-1)(N_t-1)+3$ real unknowns. Solutions to this system of equations will give the desired relative periodic solutions of the truncated system of ODEs via the expansion (4.1).

It is convenient to separate (4.4) into its linear and nonlinear parts and write it as

$$\mathbf{F}(\hat{\boldsymbol{a}}, \varphi, S, T) \;=\; \mathbf{F}_{\mathrm{L}}(\hat{\boldsymbol{a}}, \varphi, S, T) + \mathbf{F}_{\mathrm{NL}}(\hat{\boldsymbol{a}}) \;=\; \mathbf{0}, \tag{4.5}$$

where $\hat{\boldsymbol{a}}$ is a vector with components given by the coefficients $\{\hat{a}_{m,n}\}$, $\mathbf{F}_{\mathrm{L}}(\hat{\boldsymbol{a}}, \varphi, S, T)$ is a vector whose components are given by

$$\left(\mathrm{i}\left(\frac{2\pi n}{T} - \frac{\varphi}{T} - m\frac{S}{T}\right) - R + m^2(1+\mathrm{i}\nu)\right)\hat{a}_{m,n},$$

and $\mathbf{F}_{\mathrm{NL}}(\hat{\boldsymbol{a}})$ is a vector with components given by

$$(1+\mathrm{i}\mu)\sum_{m_1+m_2-m_3=m}\left(\sum_{n_1+n_2-n_3=n}\hat{a}_{m_1,n_1}\hat{a}_{m_2,n_2}\hat{a}^*_{m_3,n_3}\right).$$

Note that the components of $\mathbf{F}_{\mathrm{NL}}(\hat{\boldsymbol{a}})$ are just the coefficients in the truncated Fourier series expansion (in both space and time) of the function $(1+\mathrm{i}\mu)A|A|^2$. We remark that in defining the vector $\hat{\boldsymbol{a}}$ (and similarly for $\mathbf{F}_{\mathrm{L}}$ and $\mathbf{F}_{\mathrm{NL}}$) we are implicitly assigning an ordering on the coefficients $\{\hat{a}_{m,n}\}$ that uniquely determines an index for the components of $\hat{\boldsymbol{a}}$. Henceforth, such a convention should be understood whenever applicable. In addition, we will use the notation in (4.5) to denote both the system of complex equations (4.4) and the system of equations (4.4) split into its real and imaginary parts, as it should be clear from the context which case applies.

4.2. Symmetries of $\mathbf{F} = \mathbf{0}$. The symmetries (3.7)–(3.10) of the system of ODEs (3.6) induce symmetries of the system of nonlinear algebraic equations (4.4). Note that if $(\{\hat{a}_{m,n}\}, \varphi, S, T)$ is a solution of $\mathbf{F} = \mathbf{0}$, then for any $(\eta_1, \eta_2, \tau) \in \mathbb{T}^3$

$$(\{\mathrm{e}^{\mathrm{i}\eta_1}\hat{a}_{m,n}\}, \varphi, S, T), \tag{4.6}$$

$$(\{\mathrm{e}^{\mathrm{i}m\eta_2}\hat{a}_{m,n}\}, \varphi, S, T), \tag{4.7}$$

$$(\{\mathrm{e}^{\mathrm{i}n\tau}\hat{a}_{m,n}\}, \varphi, S, T), \tag{4.8}$$

$$(\{\hat{a}_{-m,n}\}, \varphi, -S, T), \tag{4.9}$$

are also solutions. From the continuous symmetries (4.6)–(4.8), it follows that the set of solutions to $\mathbf{F} = \mathbf{0}$ splits into orbits $\mathcal{O}_{(\hat{\boldsymbol{a}},\varphi,S,T)}$ of the symmetry group $\mathbb{T}^3$,

$$\mathcal{O}_{(\hat{\boldsymbol{a}},\varphi,S,T)} := \left\{(\eta_1, \eta_2, \tau) \cdot (\hat{\boldsymbol{a}}, \varphi, S, T) \ : \ (\eta_1, \eta_2, \tau) \in \mathbb{T}^3\right\},$$

where the action of $\mathbb{T}^3$ on a point $(\hat{\boldsymbol{a}}, \varphi, S, T)$ is defined by

$$(\eta_1, \eta_2, \tau) \cdot (\hat{\boldsymbol{a}}, \varphi, S, T) \ = \ (\{\mathrm{e}^{\mathrm{i}\eta_1}\mathrm{e}^{\mathrm{i}m\eta_2}\mathrm{e}^{\mathrm{i}n\tau}\hat{a}_{m,n}\}, \varphi, S, T). \tag{4.10}$$

That is, $\mathbb{T}^3$ acts on $\hat{\boldsymbol{a}}$ via multiplication by the matrix $\mathrm{diag}(\mathrm{e}^{\mathrm{i}\eta_1}\mathrm{e}^{\mathrm{i}m\eta_2}\mathrm{e}^{\mathrm{i}n\tau})$, and it acts trivially on (φ, S, T). Since the solutions of $\mathbf{F} = \mathbf{0}$ come in continuous families, when computing solutions to $\mathbf{F} = \mathbf{0}$ numerically we will augment the system with additional equations (and hence solve a system with equal numbers of equations and unknowns), in effect fixing a particular solution from each orbit $\mathcal{O}_{(\hat{\boldsymbol{a}},\varphi,S,T)}$.

4.3. Kernel of Jacobian Matrix at Solutions of $\mathbf{F} = \mathbf{0}$. Recall that, split into its real and imaginary parts, the system $\mathbf{F} = \mathbf{0}$ is an underdetermined system of $2(N_x - 1)(N_t - 1)$ real equations in $2(N_x - 1)(N_t - 1) + 3$ real unknowns. Thus, the kernel, $\ker(J)$, of the Jacobian matrix J of $\mathbf{F}$ is at least three-dimensional. From the $\mathbb{T}^3$-equivariance of $\mathbf{F}$ (implied by the symmetries (4.6)–(4.8)), one obtains three linearly independent vectors in $\ker(J)$ at a solution $(\hat{\boldsymbol{a}}, \varphi, S, T)$ of $\mathbf{F} = \mathbf{0}$. Such vectors result from a basis for the space of infinitesimal generators of the action (4.10) of $\mathbb{T}^3$ on the point $(\hat{\boldsymbol{a}}, \varphi, S, T)$, which can be obtained as

$$\hat{\boldsymbol{v}}_1 \ := \ \frac{\mathrm{d}}{\mathrm{d}\eta_1}\left(\{\mathrm{e}^{\mathrm{i}\eta_1}\hat{a}_{m,n}\}, \varphi, S, T\right)\Big|_{\eta_1=0} = (\{\mathrm{i}\,\hat{a}_{m,n}\}, 0, 0, 0)\,, \tag{4.11}$$

$$\hat{\boldsymbol{v}}_2 \ := \ \frac{\mathrm{d}}{\mathrm{d}\eta_2}\left(\{\mathrm{e}^{\mathrm{i}m\eta_2}\hat{a}_{m,n}\}, \varphi, S, T\right)\Big|_{\eta_2=0} = (\{\mathrm{i}m\,\hat{a}_{m,n}\}, 0, 0, 0)\,, \tag{4.12}$$

$$\hat{\boldsymbol{v}}_3 \ := \ \frac{\mathrm{d}}{\mathrm{d}\tau}\left(\{\mathrm{e}^{\mathrm{i}n\tau}\hat{a}_{m,n}\}, \varphi, S, T\right)\Big|_{\tau=0} = (\{\mathrm{i}n\,\hat{a}_{m,n}\}, 0, 0, 0)\,. \tag{4.13}$$

Split into real and imaginary parts, the above vectors $\hat{\boldsymbol{v}}_1$, $\hat{\boldsymbol{v}}_2$, and $\hat{\boldsymbol{v}}_3$ are in $\ker(J)$ at a solution $(\hat{\boldsymbol{a}}, \varphi, S, T)$ of $\mathbf{F} = \mathbf{0}$.

As previously pointed out, we will augment the system $\mathbf{F} = \mathbf{0}$ with additional equations and look for solutions of the augmented system. The additional equations should be defined so that the vectors in (4.11)–(4.13) are not in the kernel of the augmented Jacobian matrix at a solution, since a singularity of the Jacobian is usually problematic for solvers of systems of nonlinear algebraic equations. One must then confront the question of whether, at a solution of $\mathbf{F} = \mathbf{0}$, the vectors in (4.11)–(4.13) span $\ker(J)$, so that the Jacobian of the augmented system will be nonsingular at solutions. Typically this will be true, as explained next.

For a (g_0, T)-relative periodic solution $\gamma(t) \subset \mathbb{C}^N$ of a G-equivariant system of ODEs, where $g \in G$ acts on $\mathbb{C}^N$ via multiplication by a matrix N_g, define the *relative monodromy matrix* M to be

$$M = N_{g_0}\tilde{M},$$

where $\tilde{M}$ is the time T monodromy matrix along the solution. (For our problem $N_{g_0} = e^{L_{g_0}}$, where L_{g_0} is the matrix $\mathrm{diag}(\mathrm{i}\varphi + \mathrm{i}mS)$.) Thus, M is the derivative at $\gamma(0)$ of the transformation $g_0 \cdot \phi_T$ that sends $\gamma(0)$ to itself by flowing along the relative periodic solution for time T and then moving as dictated by the drift g_0. Say that γ is a *regular relative periodic solution* if the only eigenvalues of M equal to 1 are those coming from the continuous symmetries (including time translation) of the system of ODEs. Let $\mathrm{F} = 0$ denote the system of nonlinear algebraic equations whose solutions give (g_0, T)-relative periodic solutions of the system of ODEs. If γ is a (g_0, T)-relative periodic solution, then one can show that each eigenvalue λ of the relative monodromy M corresponds to an eigenvalue $-\log(\lambda)/T$ of the Jacobian matrix J of F at the solution to $\mathrm{F} = 0$ [6]. Now, J will have many eigenvalues that are not related to eigenvalues of M, but every zero eigenvalue of J does correspond to a 1 in the spectrum of M. Thus, if γ is a regular relative periodic solution, then the kernel of the Jacobian matrix of F is spanned by the infinitesimal generators of the group action. Furthermore, among ODEs with a given continuous symmetry, it is C^k-generic for all $k > 1$ that all relative periodic orbits are regular [23].

4.4. Additional Equations. When defining additional equations to augment the system $\mathbf{F} = \mathbf{0}$, we want to accomplish two objectives: first, to guarantee that solutions are not lost as a result of adding new equations; second, to derive conditions necessary so that the vectors given in (4.11)–(4.13) are not in the kernel of the Jacobian matrix of the augmented system at a solution. There are a variety of options available to accomplish these two goals. The construction we found to work best for our problem is to fix the sum of the arguments of some given sets $\Lambda_l = \{\hat{a}_{m_j^l, n_j^l}\}_{j=1}^K$, $l = 1, 2, 3$, of K nonzero coefficients by imposing the constraints

$$\sum_{j=1}^{K} \arg(\hat{a}_{m_j^l, n_j^l}) = c_l, \tag{4.14}$$

where c_1, c_2, and c_3 denote some given constants. Note that in the indexing notation used above, the superscript l is used to indicate membership of a given coefficient $\hat{a}_{m_j^l, n_j^l}$ into one of the sets Λ_1, Λ_2, or Λ_3. To verify that imposing the constraints (4.14) does not result in a loss of solutions to $\mathbf{F} = \mathbf{0}$, recall that, because of the symmetries (4.6)–(4.8), if $(\{\hat{b}_{m,n}\}, \varphi, S, T)$ is a solution to $\mathbf{F} = \mathbf{0}$, then so is $(\{\hat{a}_{m,n}\}, \varphi, S, T)$, where

$$\hat{a}_{m,n} = \mathrm{e}^{\mathrm{i}\eta_1}\mathrm{e}^{\mathrm{i}m\eta_2}\mathrm{e}^{\mathrm{i}n\tau}\hat{b}_{m,n}$$

and the element $(\eta_1, \eta_2, \tau) \in \mathbb{T}^3$ is arbitrary. Therefore, the constraints (4.14) are well defined if there exist some η_1, η_2, τ such that (for $l = 1, 2, 3$)

$$\sum_{j=1}^{K} \arg(\exp(\mathrm{i}\eta_1)\exp(\mathrm{i}m_j^l\eta_2)\exp(\mathrm{i}n_j^l\tau)\hat{b}_{m_j^l, n_j^l}) = c_l$$

or, equivalently, if a solution to the linear system

$$\begin{bmatrix} K & \sum_j m_j^1 & \sum_j n_j^1 \\ K & \sum_j m_j^2 & \sum_j n_j^2 \\ K & \sum_j m_j^3 & \sum_j n_j^3 \end{bmatrix} \begin{bmatrix} \eta_1 \\ \eta_2 \\ \tau \end{bmatrix} = \begin{bmatrix} c_1 - \sum_j \arg(\hat{b}_{m_j^1, n_j^1}) \\ c_2 - \sum_j \arg(\hat{b}_{m_j^2, n_j^2}) \\ c_3 - \sum_j \arg(\hat{b}_{m_j^3, n_j^3}) \end{bmatrix} \tag{4.15}$$

exists. But one can always assign coefficients to each set Λ_l so that the matrix in the above system of linear equations is nonsingular and therefore guarantee the existence of a unique solution to (4.15). Thus, there always exists a symmetry transformation by which it is possible to transform any solution of $\mathbf{F} = \mathbf{0}$ so that it satisfies the constraints (4.14). Hence, the constraints are well defined.

Now let $(\hat{\boldsymbol{a}}, \varphi, S, T)$ be a solution of $\mathbf{F} = \mathbf{0}$. Let J denote the Jacobian matrix of $\mathbf{F}$ augmented with the equations (4.14) and evaluated at $(\hat{\boldsymbol{a}}, \varphi, S, T)$, and let the vectors $\hat{\boldsymbol{v}}_1$, $\hat{\boldsymbol{v}}_2$, and $\hat{\boldsymbol{v}}_3$ be as in (4.11)–(4.13). Then it follows that

$$J\hat{\boldsymbol{v}}_1 = \begin{bmatrix} \mathbf{0} \\ K \\ K \\ K \end{bmatrix}, \qquad J\hat{\boldsymbol{v}}_2 = \begin{bmatrix} \mathbf{0} \\ \sum_j m_j^1 \\ \sum_j m_j^2 \\ \sum_j m_j^3 \end{bmatrix}, \qquad J\hat{\boldsymbol{v}}_3 = \begin{bmatrix} \mathbf{0} \\ \sum_j n_j^1 \\ \sum_j n_j^2 \\ \sum_j n_j^3 \end{bmatrix},$$

where $\mathbf{0} \in \mathbb{R}^{2(N_x-1)(N_t-1)}$. Thus, if the sets Λ_1, Λ_2, and Λ_3 are nonempty, and if at least one of the sums $\sum_j m_j^l$ and $\sum_j n_j^l$ are nonzero, then the vectors $\hat{\boldsymbol{v}}_1$, $\hat{\boldsymbol{v}}_2$, and $\hat{\boldsymbol{v}}_3$ will not be in the null space of J.

4.5. Identifying Minimum Time Period and Relative Equilibria. It can happen that a computed solution $(\hat{\boldsymbol{a}}, \varphi, S, T)$ to $\mathbf{F} = \mathbf{0}$ represents a relative periodic solution of the CGLE whose period T is not minimal. In such a case, there exists an integer $p > 1$ and rational numbers j and l so that

$$\tilde{T} \;=\; T/p, \qquad \tilde{S} \;=\; (S + 2\pi j)/p, \qquad \tilde{\varphi} \;=\; (\varphi + 2\pi l)/p$$

satisfy

$$\mathrm{e}^{\mathrm{i}\tilde{\varphi}} A(x + \tilde{S}, t + \tilde{T}) \;=\; A(x, t). \tag{4.16}$$

Using the expansions (3.5) and (4.1) one has that

$$\mathrm{e}^{\mathrm{i}\tilde{\varphi}} A(x + \tilde{S}, t + \tilde{T}) \;=\; \sum_m \left(\mathrm{e}^{-\mathrm{i}\frac{\varphi}{T}t} \mathrm{e}^{-\mathrm{i}m\frac{S}{T}t} \sum_n \hat{a}_{m,n} \mathrm{e}^{\mathrm{i}n\frac{2\pi}{T}t} \mathrm{e}^{\mathrm{i}\frac{2\pi(n+l+jm)}{p}} \right) \mathrm{e}^{\mathrm{i}mx},$$

so (4.16) holds only if $\hat{a}_{m,n} = 0$ whenever p does not divide $n + l + jm$. The nonzero coefficients $\hat{a}_{m,n}$ define a set $\{\tilde{a}_{m,n'}\}$, where

$$\tilde{a}_{m,(n+l+jm)/p} \;=\; \hat{a}_{m,n}$$

if p divides $n+l+jm$, giving a point $(\tilde{\boldsymbol{a}}, \tilde{\varphi}, \tilde{S}, \tilde{T})$ that corresponds to a relative periodic solution of the CGLE with minimal time period $\tilde{T}$.

Now, a relative equilibrium $A(x,t) = \mathrm{e}^{\mathrm{i}\omega_1 t}\alpha(x + \omega_2 t)$ of the CGLE satisfies the equation (1.3) defining relative periodic solutions with $(\varphi, S, T) = (-\omega_1 u, -\omega_2 u, u)$, for any $u > 0$. Using the expansion $\alpha(x) = \sum c_m \mathrm{e}^{\mathrm{i}mx}$ and such values of (φ, S, T) in the ansatz (4.1) yields that for all m, $\hat{a}_{m,0} = c_m$, and when $n \neq 0$, $\hat{a}_{m,n} = 0$. More generally, a solution to $\mathbf{F} = \mathbf{0}$ representing a relative equilibrium will have $\hat{a}_{m,n'} \neq 0$ for one index n' (not necessarily $n' = 0$) and $\hat{a}_{m,n} = 0$ when $n \neq n'$. Thus, from the computed values of $(\hat{\boldsymbol{a}}, \varphi, S, T)$ it is easy to detect when a solution is a relative equilibrium and not a relative periodic solution.

4.6. Starting Values for Solving $\mathbf{F} = \mathbf{0}$. As with almost any system of nonlinear algebraic equations, the augmented system $\mathbf{F} = \mathbf{0}$ must be solved using a method that involves iteration. This requires us to supply an initial guess as a starting point for the iterative procedure. In general, it is very important to supply initial guesses that in some sense are "close" to actual solutions of the system being solved. For our problem, we adapted the idea of searching for close returns (or recurrences) of a chaotic dynamical system and sought *relative close returns* of the truncated system of ODEs (3.6) to generate the required initial guesses.

When computing solutions $\boldsymbol{u}(t)$ of a chaotic dynamical system that are truly periodic in time (i.e., $\boldsymbol{u}(t) = \boldsymbol{u}(t+\tilde{T})$ for some time period $\tilde{T}$) it is common to search for close returns of the system, that is, integrate the system until $\boldsymbol{u}(t_1) \approx \boldsymbol{u}(t_2)$ for some times $t_1 < t_2$, to within some tolerance, and use the close return as an initial approximation to a time-periodic solution. Since for a (g,T)-relative periodic solution of the truncated system of ODEs (3.6) one has that $|a_m(t)| = |a_m(t+T)|$ (cf. equation (3.15)), we sought sets of coefficients $\{a_m(t)\}$ for which

$$|a_m(t_1)| \approx |a_m(t_2)|$$

for some times $t_1 < t_2$. Given a measure δ of desired closeness, the truncated system of ODEs (3.6) was integrated starting with some random set $\{a_m(0)\}$ of coefficients until times $t_1 < t_2$ were found for which

$$\max_m \left| 1 - \frac{|a_m(t_2)|}{|a_m(t_1)|} \right| \leq \delta.$$

The initial value T_0 for the time period was then set to $T_0 = t_2 - t_1$ and a least squares solution over φ and S to the system

$$a_m(t_1) = \mathrm{e}^{\mathrm{i}\varphi}\mathrm{e}^{\mathrm{i}mS}a_m(t_2)$$

was taken as an initial value $g_0 = (\varphi_0, S_0)$ for the drift. Once such a relative close return was identified, initial values for the Fourier coefficients $\{\hat{a}_{m,n}\}$ were generated. We set (cf. equation (4.1))

$$\mathrm{e}^{\mathrm{i}(\varphi_0/T_0)t}\mathrm{e}^{\mathrm{i}m(S_0/T_0)t}a_m(t) = \sum_n \hat{a}_{m,n}\mathrm{e}^{\mathrm{i}n(2\pi/T_0)t}$$

and used the Fast Fourier Transform (FFT) algorithm to compute the initial guess for the coefficients $\{\hat{a}_{m,n}\}$.

4.7. Numerical Solution of $\mathbf{F} = \mathbf{0}$. The augmented system $\mathbf{F} = \mathbf{0}$ was solved using the nonlinear least squares solver `lmder` from the MINPACK software package [47]. This solver is an implementation of the Levenberg-Marquardt method [38, 42, 48] for solving nonlinear least squares problems. The solver `lmder` was chosen because it performed better on the CGLE problem addressed in this study than the other alternatives considered, namely Newton's method with a line search [16] and a modification of Powell's hybrid method [47, 51] for solving nonlinear equations. A brief discussion on the performance of these other solvers on our problem is given at the end of this section.

To use the solver `lmder` we need to provide a routine that returns the value of $\mathbf{F}$ (augmented) evaluated at a given point $(\hat{\boldsymbol{a}}, \varphi, S, T)$. Computing $\mathbf{F}_{\mathrm{L}}(\hat{\boldsymbol{a}}, \varphi, S, T)$, as defined in (4.5), is straightforward. As for $\mathbf{F}_{\mathrm{NL}}(\hat{\boldsymbol{a}})$, note that since it is a vector

with components given by the coefficients in the truncated (space-time) Fourier series expansion of $(1+\mathrm{i}\mu)A|A|^2$, one can compute it using the FFT algorithm. This is a standard procedure for computing nonlinear terms in spectral discretizations, see for example [8], and is briefly detailed here. Let x_j and t_l denote grid-point values of the spatial variable x and time variable t, respectively, in physical space. To obtain the Fourier coefficients of $A|A|^2$, the inverse FFT algorithm was used to compute the values $A(x_j,t_l)$, given the coefficients $\{\hat{a}_{m,n}\}$. In order to avoid aliasing error when computing the convolution sums in (4.4) via the FFT algorithm, the coefficients $\{\hat{a}_{m,n}\}$ were padded with zeros to obtain a set $\{\tilde{a}_{m',n'}\}$, where $m'=-N_x,\ldots,N_x$, $n'=-N_t,\ldots,N_t$, and $\tilde{a}_{m',n'}$ was equal to $\hat{a}_{m',n'}$ if $|m'|<N_x/2$ and $|n'|<N_t/2$, and 0 otherwise. (Based on the 3/2 rule for dealiasing quadratic products [8], the number of modes $\{\tilde{a}_{m',n'}\}$ used are sufficient for dealiasing a cubic nonlinearity.) The inverse FFT was done using the coefficients $\{\tilde{a}_{m',n'}\}$. Then, the pointwise products $A(x_j,t_l)|A(x_j,t_l)|^2$ were computed in physical space. Finally, the FFT algorithm was used to compute the Fourier coefficients of $A|A|^2$. At this point only those coefficients whose index (m',n') satisfied $|m'|<N_x/2$ and $|n'|<N_t/2$ were retained. The FFTW software package [25] was used in our computations.

Some points are worth mentioning regarding the additional equations (4.14). First, pairs of indices $\{(m_j^l,n_j^l)\}_{j=1}^K$, $l=1,2,3$, were associated with the sets Λ_1, Λ_2, and Λ_3 so that the linear system in (4.15) was guaranteed to have a solution. Second, the values of c_1, c_2, and c_3 in (4.14) were set to the sum of the arguments of the coefficients corresponding to the current approximation to a solution. That is, each time $\mathbf{F}$ augmented was evaluated, the equations (4.14) were satisfied exactly. This is appropriate since the justification for using these additional equations does not depend on the specific values of c_1, c_2, and c_3. Finally, which elements were in the sets Λ_1, Λ_2, and Λ_3 depended not only on the pairs of indices associated with them, but also on the value of the coefficients corresponding to the current approximation to a solution. Coefficients whose absolute value was below a given tolerance, usually 10^{-5}, were excluded from the sets.

The MINPACK software package makes use of the Jacobian matrix of the system being solved (or some approximation to it) and provides the option of computing the Jacobian using finite differences or (analytically) via a user supplied routine. We chose the latter option. Note that it is straightforward to compute the derivatives of $\mathbf{F}_{\mathrm{L}}(\hat{\boldsymbol{a}},\varphi,S,T)$ with respect to φ, S, T, and the real and imaginary parts of the coefficients $\{\hat{a}_{m,n}\}$. On the other hand, computing the derivatives of $\mathbf{F}_{\mathrm{NL}}(\hat{\boldsymbol{a}})$ with respect to the real and imaginary parts of the coefficients $\{\hat{a}_{m,n}\}$ directly from the convolution sums in (4.4) is potentially an error-prone process. However, one can use the directional derivative $A^2V^*+2|A|^2V$ of the function $A|A|^2$ in the direction of a perturbation $V(x,t)$ to $A(x,t)$ to compute the product of a given vector $\hat{\boldsymbol{v}}$ (whose components are the real and imaginary parts of the Fourier coefficients $\{\hat{v}_{m,n}\}$ of $V(x,t)$) and the Jacobian matrix of $\mathbf{F}_{\mathrm{NL}}$ evaluated at a point $\hat{\boldsymbol{a}}$. By virtue of the discretization used, this matrix-vector product has components given by the coefficients in the truncated Fourier series expansion (in both space and time) of the function $(1+\mathrm{i}\mu)(A^2V^*+2|A|^2V)$. Hence, the matrix-vector product can be computed using a procedure analogous to that for computing $\mathbf{F}_{\mathrm{NL}}(\hat{\boldsymbol{a}})$, which was outlined earlier in this section. The difference here is that one has two sets of Fourier coefficients, $\{\hat{a}_{m,n}\}$ and $\{\hat{v}_{m,n}\}$, and that the pointwise products to be computed in physical space are for the function $A^2V^*+2|A|^2V$. The Jacobian matrix of $\mathbf{F}_{\mathrm{NL}}$ can thus be computed by substituting for $\hat{\boldsymbol{v}}$ the standard basis vectors in $\mathbb{R}^{2(N_x-1)(N_t-1)}$.

As for the measure of closeness δ used to identify relative close returns, setting $\delta \geq 0.5$ worked well, but choosing smaller values of δ usually proved unsuccessful in identifying relative close returns. We used the value $\delta = 0.5$, chosen experimentally, and the initial guesses generated from the resulting relative close returns were frequently good starting points for the solver `lmder`. When searching for relative close returns, we also specified a range $[p_1, p_2]$ for the initial time period T_0. If δ was chosen to be too large, then most relative close returns would end up having period $T_0 = p_1$. With $\delta = 0.5$, the search for relative close returns was always successful, but also resulted in relative close returns with different values within the interval $[p_1, p_2]$ for the initial time period T_0. We remark that the use of random initial data (i.e., not resulting from a relative close return), even with the spectral profile of a typical trajectory of the truncated system of ODEs, was unsuccessful in generating solutions with any of the nonlinear equations solvers.

Initially, the system of nonlinear algebraic equations was solved using values of $N_x = 32$ and $N_t = 48$ (giving a total of 2,917 real variables). For this value of N_x, the decay in the spatial spectra of the relative close returns was around five orders of magnitude. This proved to be sufficient in order to have well defined solutions in the sense that once a solution was found, continuing from it with $N_x > 32$ posed no challenge for the nonlinear equations solver and in a very small number of iterations it converged to the same solution. The value $N_t = 48$ was chosen to allow for a relatively large range of time periods. If the solver `lmder` converged to a solution of $\mathbf{F} = \mathbf{0}$, then we verified whether the solution had minimal time period using the criteria from § 4.5. If not, a new set of Fourier coefficients was defined and the values of T, S, and φ modified in order to obtain a solution with minimal time period. Then the values of N_x and N_t were increased, if necessary, to have a good decay (around eight or more orders of magnitude) in the spectra of the solution. At this point, using Newton's method to solve the system of nonlinear algebraic equations worked well: only 2–4 iterations were required for convergence. Finally, the solution to $\mathbf{F} = \mathbf{0}$ was used as an initial condition and the truncated system of ODEs (3.6) was integrated to verify that we indeed had a relative periodic solution of the system of ODEs (and thus of the CGLE).

As for the other solvers considered, the performance of Newton's method with a line search [16] was, in general, unsatisfactory for our problem. The typical behavior was that, as the iterations progressed, the line search parameter became very small and no significant change in the iterates nor reduction in the value of $||\mathbf{F}||_2^2$ was achieved. The MINPACK solver for systems of nonlinear algebraic equations, `hybrj`, was also tried on our problem. It is an implementation of a modification of Powell's hybrid method [47, 51] for solving nonlinear equations. The solver `hybrj` often terminated without converging to a solution of $\mathbf{F} = \mathbf{0}$ nor to a minimum of $\mathbf{F}^{\mathrm{T}}\mathbf{F}$ for which $\mathbf{F} \neq \mathbf{0}$.

5. The Relative Periodic Solutions.

5.1. Dynamical Properties. Using the procedure described in § 4, 77 distinct relative periodic solutions were found for the CGLE (1.1) with the parameter values $R = 16$, $\nu = -7$, and $\mu = 5$. The solutions display a wide variety of dynamical and spatial properties, some of which are summarized in Appendix A, Table A.1, and illustrated in Figures 5.1 and 5.2. In Table A.1 the solutions are sorted by increasing period, with the periods in the range $0.02 < T < 0.46$. The solutions are given an identifying number in the left column corresponding to their position in the list.

The Lyapunov exponents of the solutions were computed from the eigenvalues of the relative monodromy matrix defined in § 4.3. As a consequence of the continuous

symmetries and the flow direction, each relative periodic solution has three zero exponents [2]. This was confirmed numerically. Figure 5.1(a) shows the largest Lyapunov exponent of each solution plotted against the corresponding time period, while Figure 5.1(b) shows the total instability. The horizontal dotted line on each graph gives the value of the corresponding dynamical quantity computed for a typical trajectory, which is assumed to be characteristic of the main attractor (cf. § 3.4).

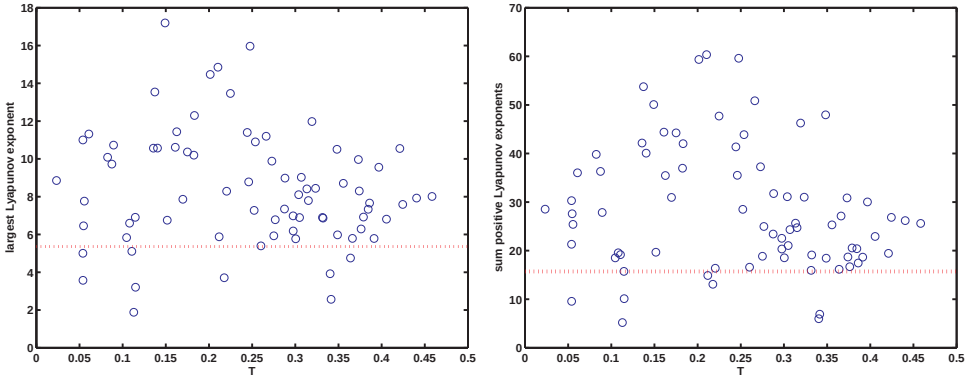

(a) (b)

FIG. 5.1. *(a) Largest Lyapunov exponent vs. period and (b) total instability vs. period for relative periodic solutions. Mean value for typical solutions denoted by horizontal dotted line.*

Figure 5.2 shows the unstable dimension of each solution plotted against the period. As noted in § 3.3, each relative periodic solution represents an invariant three-torus in the CGLE semiflow, and so, for example, a relative periodic solution with five positive Lyapunov exponents corresponds to a flow invariant three-torus with a 5-dimensional unstable manifold. The unstable dimension variability of the system is clearly illustrated in Figure 5.2. We have been unable to associate the various values of unstable dimension with specific regions of the main attractor, but the high dimensionality makes a clear geometric picture of the attractor very difficult to obtain.

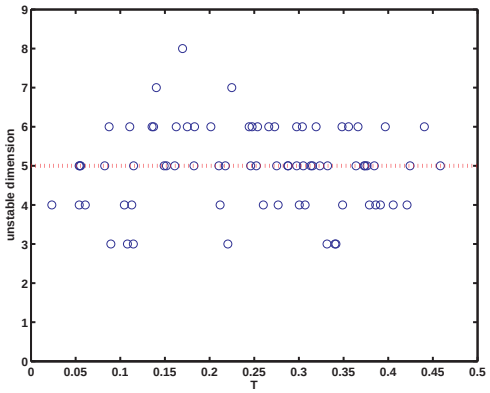

FIG. 5.2. *Unstable dimension vs. period for relative periodic solutions. Value for typical solutions denoted by horizontal dotted line.*

As seen in Table A.1, the solutions possess a wide variety of space shifts S and

phase shifts φ. A relative periodic solution can be the "k^{th} root" of true periodic solution if $A(x, kT) = A(x, 0)$ for some integer k. This happens exactly when $k\varphi$ and kS are both integer multiples of 2π and corresponds to the dynamical situation of a rational flow (every orbit is periodic) on the invariant three-torus. To test for this possibility we computed the best rational approximation to each $\varphi/(2\pi)$ and $S/(2\pi)$ using the MATLAB function `rationalize`. For no solutions did the rational approximations of $\varphi/(2\pi)$ and $S/(2\pi)$ share the same denominator, and in most cases the denominators of the rational approximates were on the order of several hundred. These results indicate that, at least for moderate size k, the computed relative periodic solutions are not k^{th} roots of true periodic solutions and that the dynamics on the invariant three-tori are either an irrational flow or else a periodic flow with long period.

The semilog plots of the temporal and spatial power spectra of all the computed relative periodic solutions are approximately linear, indicating near exponential decay in these spectra. Figure 5.4 in § 5.2 shows plots of the spectra for solution 14. The exponential decay reflects the fact that solutions on the CGLE attractor are C^ω in time [52] and space [21]. In addition, the temporal spectra indicate that none of the 77 computed relative periodic solutions are coherent structures.

5.2. Properties of Specific Solutions. To give an idea of the character of the solutions we describe a few in some detail. The first relative periodic solution found, identified as solution 14 in Table A.1, is the least unstable among our collection of relative periodic solutions. The time evolution of solution 14, represented as curves on the plane with coordinates defined by the real and imaginary parts of $A(x, t)$ at different times in the interval $[0, T]$, is displayed in Figure 5.3. The nontrivial time

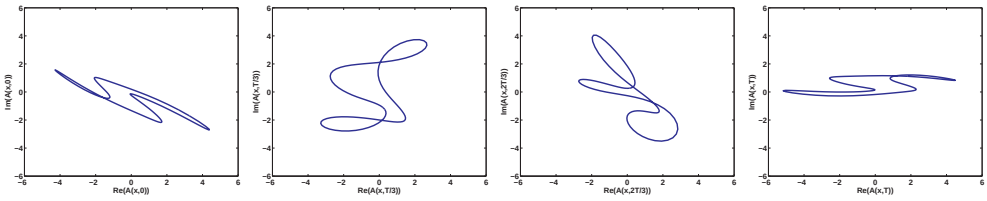

FIG. 5.3. *Imaginary vs. real part of solution 14 at times* $t = 0, T/3, 2T/3, T$. *Solution has phase shift* $\varphi = 2.61$. *Click here for movie of time evolution.*

behavior of the solution (i.e., the excitation of multiple temporal frequency modes) is apparent from these curves. For single-frequency solutions $A(x, t) = B(x)e^{i\omega t}$ and generalized traveling waves $A(x, t) = \rho(x - vt)e^{i\phi(x-vt)}e^{i\omega t}$, where ω is some single frequency, plots of this kind at different times would show, except for a rotation, the same curve. It is clear, then, that solution 14 is not of either of these types. Note also that the curve at time $t = T$ differs from that at time $t = 0$ because of the rotation of the complex field $A(x, 0) \to e^{i\varphi}A(x + S, T)$. The spectra of solution 14 are displayed in Figure 5.4, where one can also observe the multiple modes active in the temporal spectrum of the solution.

Another of the solutions with total instability less than typical, listed as solution 16 in Table A.1, has period and drift close to those of solution 14. However, solution 16 has stabilizer $C(1, 2)$ (cf. § 3.2), that is, it satisfies $A(x, t) = -A(x + \pi, t)$. This property is apparent from the symmetry in each of the curves representing the time evolution of solution 16, displayed in Figure 5.5. We will come back to solutions 14 and 16 in § 5.3, where an apparent relationship between these and several other solutions is explored.

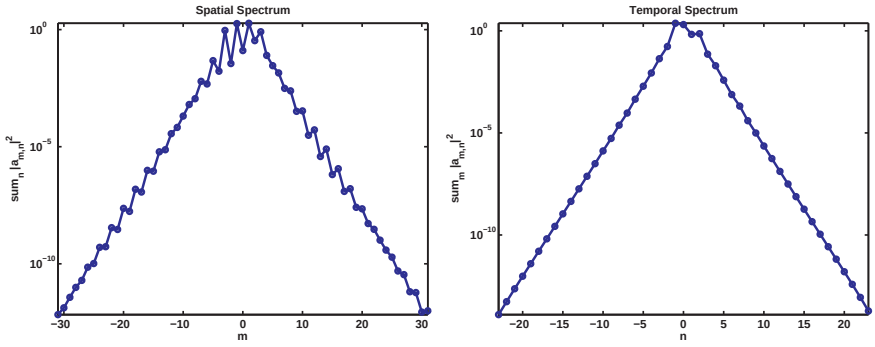

FIG. 5.4. *Spectra of solution 14.*

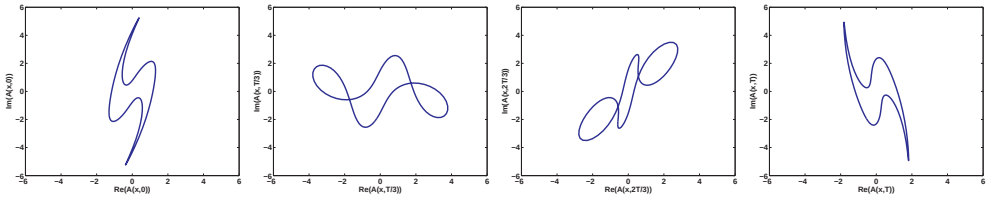

FIG. 5.5. *Imaginary vs. real part of solution 16 at times* $t = 0, T/3, 2T/3, T$. *Solution has phase shift* $\varphi = 2.72$. *It satisfies* $A(x,t) = -A(x+\pi,t)$. *Click here for movie of time evolution.*

Contour plots of the absolute value of a relative periodic solution provide a way of visualizing periodicity in time coupled with the shift S in space. Figure 5.6 shows one such plot for one of the most unstable among the relative periodic solutions found, listed as solution 20 in Table A.1. The absolute value of the solution has been plotted over two space and four time intervals. Moving vertically (in time) and horizontally (in space) allows us to observe periodicity in time, after taking into account the shift S in space. From the contours of $|A|$ one can also locate points in space-time where the magnitude of A vanishes (the darkest shaded regions (in blue) in Figure 5.6). The time evolution of solution 20 is shown in Figure 5.7. To view the time evolution of several other relative periodic solutions, click on the following red links: solution 8, solution 24, and solution 26.

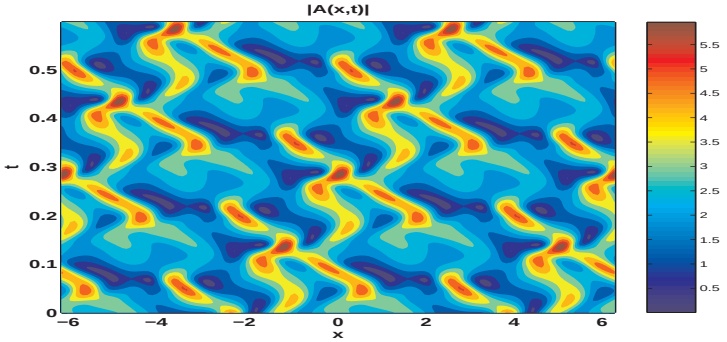

FIG. 5.6. *Contours of* $|A(x,t)|$ *for solution 20,* $x \in [-2\pi, 2\pi]$, $t \in [0, 4T]$. *Solution has space shift* $S = 1.27$.

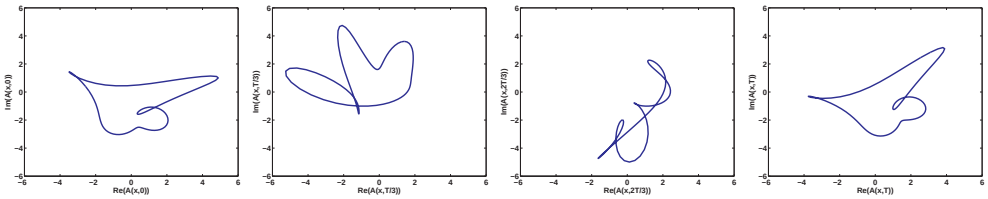

FIG. 5.7. *Imaginary vs. real part of solution 20 at times* $t = 0, T/3, 2T/3, T$. *Solution has phase shift* $\varphi = 5.81$. *Click here for movie of time evolution.*

Finally, several other relative periodic solutions have nontrivial $\mathbb{T}^2$-stabilizers and some are even or odd about certain points in the spatial domain. For instance, Figure 5.8 displays contour plots of the real and imaginary parts and the absolute value of a relative periodic solution having all these properties. The solution, identified as solution 15 in Table A.1, has total instability close to that of a typical trajectory. The drift and period of solution 15 are close to those of solutions 14 and 16, but the unstable dimension of each of these solutions is different. Like solution 16, solution 15 has stabilizer $C(1,2)$. In addition, solution 15 is odd about $x = \pi$ and even about $x = \pi/2, 3\pi/2$. Since solution 15 has stabilizer $C(1,2)$, it is also a relative periodic solution with period T and drift $(\tilde{\varphi}, \tilde{S}) = (\varphi + \pi, S + \pi)$. The space shift S of solution 15 is (numerically) equal to π, so it follows that its absolute value is (truly) periodic in time, with time period T. All these properties of solution 15 can be observed from the contour plots in Figure 5.8.

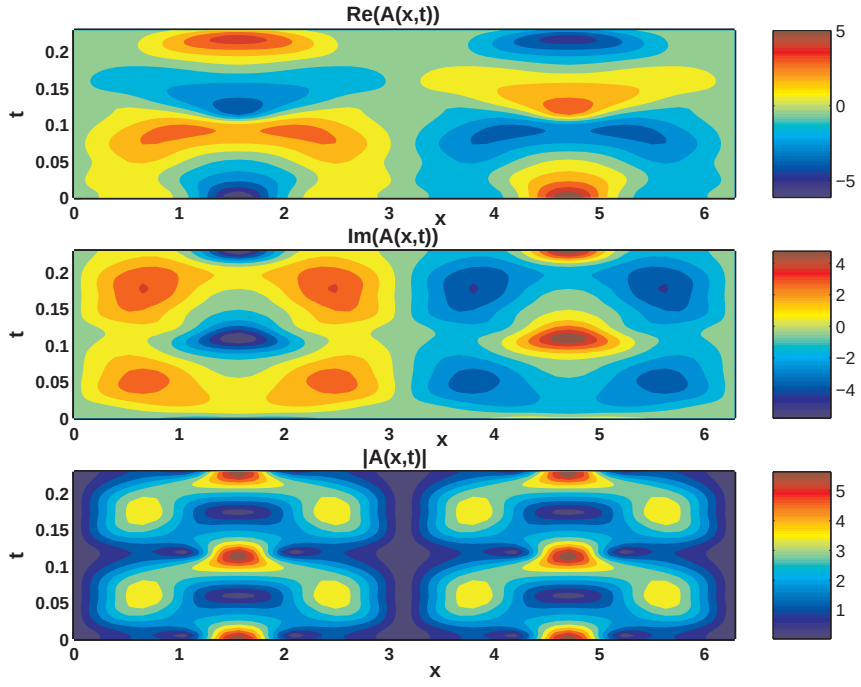

FIG. 5.8. *Contour plots for solution 15,* $x \in [0, 2\pi]$, $t \in [0, 2T]$. *Solution satisfies* $A(x,t) = -A(x+\pi, t)$ *and* $|A(x,t)| = |A(x, t+T)|$. *It is odd about* π *for* $x \in [0, 2\pi]$, *even about* $\pi/2$ *for* $x \in [0, \pi]$, *and even about* $3\pi/2$ *for* $x \in [\pi, 2\pi]$.

The other relative periodic solutions with nontrivial $\mathbb{T}^2$-stabilizers are solutions 3 and 9, which have stabilizers $C(1,2)$ and $C(1,3)$, respectively. Solutions 4 and 10 are even about $x = \pi$ and have a space shift S (numerically) equal to π. The latter results in the absolute value of each of these solutions being periodic in time with period $2T$. Such properties of solutions 3, 4, 9, and 10 can be seen from Figures 5.9–5.11. We remark that solutions 3, 9, and 10 are more unstable than typical trajectories, whereas solution 4 is among the least unstable of the solutions found.

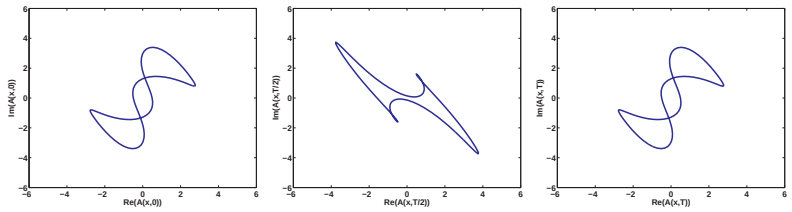

FIG. 5.9. *Imaginary vs. real part of solution 3 at times $t = 0, T/2, T$. Solution satisfies $A(x,t) = -A(x+\pi,t)$. Click here for movie of time evolution.*

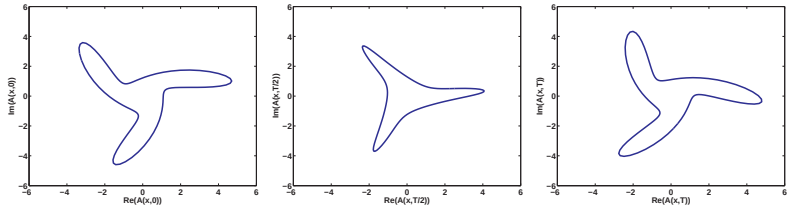

FIG. 5.10. *Imaginary vs. real part of solution 9 at times $t = 0, T/2, T$. Solution satisfies $A(x,t) = e^{i2\pi/3}A(x+2\pi/3,t)$. Click here for movie of time evolution.*

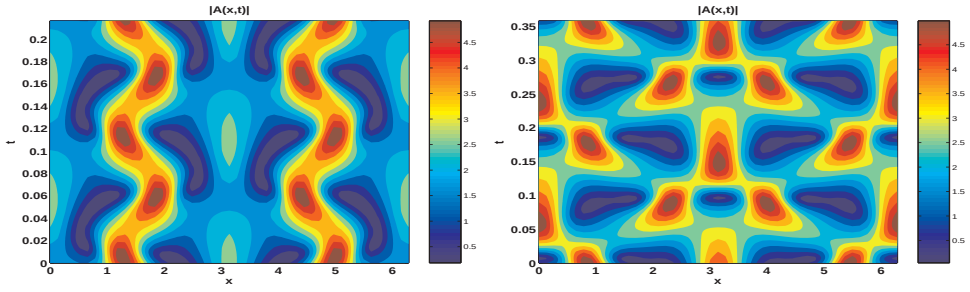

(a) (b)

FIG. 5.11. *Contours of $|A(x,t)|$ for solutions (a) 4 and (b) 10, $x \in [0, 2\pi]$, $t \in [0, 4T]$. Each solution is even about $x = \pi$ and satisfies $|A(x,t)| = |A(x,t+2T)|$.*

5.3. Instability and a Family of Solutions. There are several features of the instability of the collection of relative periodic solutions that are apparent from Figures 5.1 and 5.2: the largest Lyapunov exponent and total instability of most of the relative periodic solutions are larger than those of a typical trajectory, and in contrast, the unstable dimensions are nearly evenly distributed about the typical value. In addition, the periods of the relative periodic solutions with instability less

than typical in Figure 5.1 are clustered around what appear to be multiples of a single fundamental period.

More specifically, if $T_f = 0.054$, then the seven relative periodic solutions whose largest Lyapunov exponent and total instability are less than typical have periods close to one of T_f, $2T_f$, $4T_f$, and $6T_f$. As will be discussed below, the drifts (φ, S) of the corresponding solutions are also approximate integer multiples. This suggests that these least unstable relative periodic solutions arose via a sequence of period-multiplying bifurcations and that the resulting collection of solutions are members of a low instability (and thus high traffic) region of the main attractor, which is structured around a three-torus that projects in the reduced flow to a loop with the fundamental period T_f. Further evidence for this proposed structure is the observed repeated appearance in typical trajectories of sequences of patterns from the low instability solutions. The role of R in the equations (3.6) makes it clear that, in general, instability will increase with increasing R. Thus, low instability orbits could be continuations of solutions present for smaller values of R. This conjectured attractor structure and bifurcation scheme should certainly be investigated in further detail.

In the initial phases of this investigation we have found a collection of solutions that clearly fit together in a dynamical family. The family contains four of the seven solutions with total instability less than typical and, in fact, consists of four of the five solutions with least total instability. The family splits into the pair 14/16, which have periods approximately $2T_f$, and the pair 58/59, which have periods approximately $6T_f$. The elements of a pair have very similar (φ, S, T), and all these values for the pair 58/59 are close to three times those of pair 14/16. Solutions 14 and 16 are distinguished from each other by their unstable dimensions of 4 and 5, respectively. Solutions 58 and 59 both have unstable dimension of 3, but they differ in their unstable Floquet spectrum (i.e., the eigenvalues of the relative monodromy matrix with magnitude greater than one). In this portion of the spectrum, both solutions have a conjugate pair of complex eigenvalues, but the remaining real eigenvalue is positive for solution 58 and negative for solution 57. Thus, they have opposite Lefschetz indices as fixed points of their Poincaré map and hence the available information is consistent with solutions 58 and 59 arising together in an equivariant period-tripling bifurcation.

All four of the solutions in the family have similar appearing pattern evolution, and indeed, this is one of the features that brought them to our attention. In particular, solution 16 has stabilizer $C(1,2)$ and thus satisfies $A(x+\pi, t) = -A(x, t)$, while the other three solutions approximately have this symmetry. To investigate these "near symmetries", recall from § 3.2 that a solution has a $C(1,2)$ stabilizer exactly when its spatial Fourier coefficients (a_m) satisfy $a_m = 0$ for all even m. Thus, for each of the solutions we plotted the magnitude of the even and odd parts of the power spectrum using

$$d_0(t) = \sqrt{\sum |a_{2k}(t)|^2}, \qquad d_1(t) = \sqrt{\sum |a_{2k+1}(t)|^2}.$$

The results are shown in Figure 5.12(a), which clearly shows the strong similarities in the evolution of $d_1(t)$ and the differences in $d_0(t)$ among the members of the family. Furthermore, the magnitude of $d_1(t)$ is significantly larger than that of $d_0(t)$, confirming the presence of the approximate stabilizer. As further confirmation of the similarities in the evolution of the coefficients $a_{2k+1}(t)$ for members of the family, we show in Figure 5.12(b) the projection of the solutions onto the three-dimensional space with coordinates $(|a_{-1}(t)|, |a_1(t)|, |a_3(t)|)$ (these are the three $a_{2k+1}(t)$ with largest magnitude). We confirmed comparable similarities among the evolution of

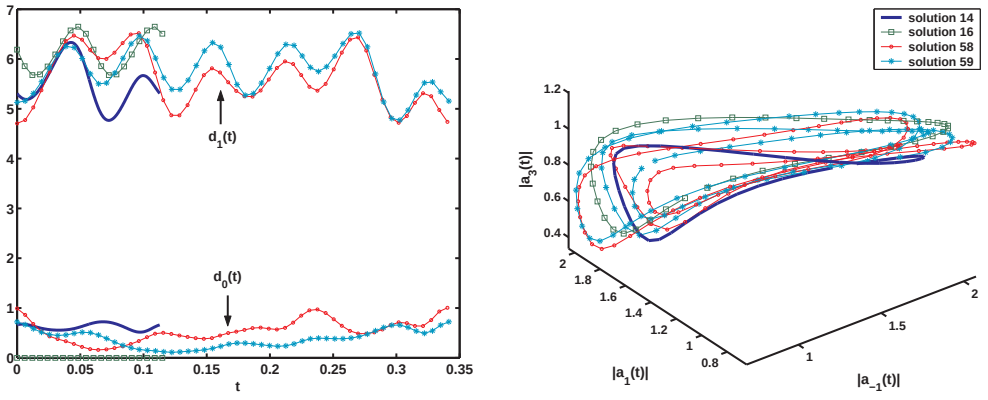

(a) (b)

FIG. 5.12. *(a) Magnitude of even ($d_0(t)$) and odd ($d_1(t)$) parts of power spectrum for solutions 14, 16, 58, 59. (b) Projection of time evolution onto three-dimensional space with coordinates* $(|a_{-1}(t)|, |a_1(t)|, |a_3(t)|)$.

the other $|a_{2k+1}(t)|$. Figure 5.12(b) also shows the pair 58/59 traversing the other solutions three times.

To put these findings in a more geometric context, we consider a direct sum decomposition of the space $\mathcal{C}$ into its odd and even pieces. More precisely, let $F_0 = \{(a_m) : a_m = 0 \text{ if } m \text{ is even}\}$ and $F_1 = \{(a_m) : a_m = 0 \text{ if } m \text{ is odd}\}$. Thus, $F_0 = \mathrm{Fix}(C(1,2))$, $F_1 = \mathrm{Fix}(C(0,2))$, and $\mathcal{C} = F_0 \oplus F_1$. Further, for $i = 0, 1$, the L^2-distance of $(a_m(t))$ to F_i is $d_i(t)$, and so Figures 5.12(a) and 5.12(b) demonstrate that the projections of the family of solutions onto F_0 are all approximately equal, and that the time evolution of the distances to F_1 are all approximately the same. In other words, the family of solutions comes very close to lying in the generalized cylinder $\Lambda \times F_1$, where $\Lambda \subset F_0$ is the full relative periodic orbit of solution 16 (i.e., its invariant three-torus), and so the bifurcations that (presumably) created these solutions respected this cylinder. Since the values of d_1 are consistently larger than those of d_0, the solutions are evolving near this cylinder reasonably close to the F_1 subspace.

Under the Fourier transform, the decomposition $\mathcal{C} = F_0 \oplus F_1$ corresponds to a decomposition $\mathcal{S} = F_0' \oplus F_1'$, where for $\alpha \in \mathcal{S}$ the projections onto F_0' and F_1' are given by $(1/2)(\alpha(x) - \alpha(x+\pi))$ and $(1/2)(\alpha(x) + \alpha(x+\pi))$, respectively. Thus, within the family the evolutions of $(1/2)(A(x,t) - A(x+\pi,t))$ are all very similar while those of $(1/2)(A(x,t) + A(x+\pi,t))$ differ.

The existence in the family of a pair with $T \approx 2T_f$ and a pair with $T \approx 6T_f$ raises the question of solutions with $T \approx T_f$ and $T \approx 4T_f$. The question of solutions with $T \approx T_f$ asks whether the pair 14/16 is itself the result of a period doubling bifurcation. Solution 4 has $T \approx T_f$ and it, along with the family, constitutes the five solutions with the least total instability. Using its drift and following it for two of its time periods, solution 4 satisfies $A_4(x,0) = \exp(5.868\mathrm{i})A_4(x, 0.108)$. On the other hand, shifting the drift of solution 16 by its stabilizer yields for one time period the very similar

$$A_{16}(x,0) = \exp(5.857\mathrm{i})A_{16}(x, 0.114). \tag{5.1}$$

Thus, in terms of its drift, period, and total instability solution 4 fits in with the

family, but it lacks the near symmetries that characterize the family and is located nowhere near the family's cylinder. The situation for solutions with $T \approx 4T_f$ is somewhat similar. After reducing mod 2π, the drift and period of solutions 30 and 31 are approximately twice those of solution 16 as given in (5.1). Thus, while the seven solutions with total instability less than typical have drifts and periods in (approximate) integer multiples, only four of the solutions show clear signs of being related by well understood bifurcations.

5.4. Weighted Averages of Observables. As mentioned in the introduction, the unstable periodic orbits embedded in a chaotic attractor can be used to approximate statistical averages that characterize the long-term dynamics of the system [13, 14, 62]. In an initial effort to investigate the usefulness of the relative periodic solutions in this regard, we use a weighted averaging scheme proposed in [62] for systems for which a symbolic dynamics is not known.

A given quantity Φ_{typ} attached to a typical trajectory is approximated by

$$\Phi_{\text{typ}} \approx < \Phi >_N := \sum_{i=1}^{N} p_i \Phi_i, \tag{5.2}$$

where

$$p_i = \frac{\frac{1}{\text{SL}_i}}{\sum_{k=1}^{N} \frac{1}{\text{SL}_k}} ,$$

Φ_i is the value of the quantity Φ computed for the i-th periodic solution, and SL_i is the sum of the positive Lyapunov exponents of the i-th periodic solution. The value $1/\text{SL}_i$ approximates the fraction of time that a typical trajectory spends in a neighborhood of the i-th periodic solution.

The quantities Φ we compute are: the largest Lyapunov exponent λ_1; the Lyapunov dimension $\text{D}_\text{L} = j + (\sum_{i=1}^{j} \lambda_i)/|\lambda_{j+1}|$, where $\lambda_1 \geq \lambda_2 \geq \ldots \geq \lambda_m$ are the Lyapunov exponents and j is the largest integer such that $\sum_{i=1}^{j} \lambda_i \geq 0$; the time average of the Ginzburg-Landau energy functional, $\text{E} = \frac{1}{T}\int_0^T \int_0^{2\pi} (-R|A|^2 + |\partial A/\partial x|^2 + |A|^4/2)\,\mathrm{d}x\,\mathrm{d}t$; the time average of the L^2-norm of the vector field that defines the CGLE, $L^2\text{-VF} = \frac{1}{T}\int_0^T (\int_0^{2\pi} |\, RA + (1+\mathrm{i}\nu)\partial^2 A/\partial x^2 - (1+\mathrm{i}\mu)A|A|^2\,|^2\,\mathrm{d}x)^{1/2}\mathrm{d}t$; and the time average of the L^2-norm of a solution $A(x,t)$ of the CGLE, $L^2\text{-A} = \frac{1}{T}\int_0^T (\int_0^{2\pi} |A|^2\,\mathrm{d}x)^{1/2}\mathrm{d}t$. Table 5.1 summarizes the results obtained using the $N = 77$ relative periodic solutions found. (We remark that the rest point $\mathbf{0}$ and the plane waves (cf. Section 3.4) were not included in the computation of the weighted averages.) From the relative errors (fourth column in Table 5.1) one could say that, except for the value of λ_1, the approximations obtained are quite good.

Φ	Φ_{typ}	$< \Phi >_{77}$	$\left\lvert\frac{\Phi_{\text{typ}} - <\Phi>_{77}}{\Phi_{\text{typ}}}\right\rvert$
λ_1	5.3573	6.9130	0.2940
D_L	11.5216	11.5707	0.0043
E	-237.4924	-247.0737	0.0403
L^2-VF	280.0915	292.6268	0.0448
L^2-A	6.3152	6.3763	0.0097

TABLE 5.1
Comparison between Φ_{typ} and approximation (5.2).

While these initial results are promising, a detailed investigation of the predictive value of the relative periodic solutions is warranted. For example, other averaging schemes which do not require knowledge of symbolic dynamics, such as those presented in [17, 18], should also be considered. Another question concerns the role that unstable dimension variability played in the computation of the trajectory averages Φ_{typ} since, as discussed in [54], convergence to erroneous values for statistical averages computed from long-time simulations is a possibility in the presence of unstable dimension variability. As for the relative periodic solutions, since they are computed using the expansions (3.5) and (4.1) (as opposed to integrating the system of ODEs (3.6)) we do not expect unstable dimension variability to have had an adverse effect in the computation of the values Φ_i.

5.5. The Iterative Solver and Dynamical Properties of Solutions. With the rather large range of stability properties exhibited by our collection of relative periodic solutions, it is interesting to consider whether these properties impact the ability of the nonlinear equations solver to converge to solutions of $\mathbf{F} = \mathbf{0}$. The 77 relative periodic solutions listed in Table A.1 resulted from 350 runs performed using the nonlinear least squares solver `lmder` and relative close returns (with a measure of closeness of $\delta = 0.5$) as starting values. In total, 146 of the 350 runs resulted in convergence to solutions of $\mathbf{F} = \mathbf{0}$ (this count includes convergence to the 77 distinct relative periodic solutions, runs that converged again to these solutions, and two runs that yielded single-frequency solutions of the CGLE), and 204 runs converged to minima of $\mathbf{F}^{\mathrm{T}}\mathbf{F}$ for which $\mathbf{F} \neq \mathbf{0}$. For those runs that converged to solutions of $\mathbf{F} = \mathbf{0}$, the final value of $||\mathbf{F}||_2$ was on the order of 10^{-9} or smaller. The total number of iterations taken by the solver `lmder` ranged between 10 and 300.

For solutions with periods in the range $0.40 < T < 0.46$, the value $N_t = 64$ (instead of $N_t = 48$; see § 4.7) was required to obtain well defined solutions, in the sense that the decay in the temporal spectra of the solutions found was around five orders of magnitude. For a generic compact attractor there will be finitely many relative periodic orbits in any finite range of periods. Of the total number of runs performed with the solver `lmder`, the last 55 yielded three new solutions. This gives around a 5.4% return on the number of new solutions found from the last set of runs, which suggests that we were approaching the point where no new solutions with periods less than 0.46 could be found with our choice of solution method. This assertion is difficult to prove, however, based only on empirical testing.

Because we solve the equations (4.4) using starting values derived from relative close returns of the system (3.6) coming from random initial data, the method we use is biased towards finding relative periodic solutions on the main attractor. Nonetheless, there is no reason to expect the iterative solver to respect the dynamics of the CGLE, so solutions disjoint from the main attractor are certainly possible. However, there do seem to be quantities associated with the CGLE dynamics that are, in certain cases, connected to the solver behavior.

Solution 14 (shown in Figure 5.3) was by far the most frequently found by the solver, with convergence to it 25 times out of the 146 runs that converged to solutions. It was also the first solution found as well as being the least unstable solution by both measures shown in Figure 5.1. The instability of a relative periodic solution can be connected (cf. § 4.3) with the eigenvalues of the Jacobian matrix of $\mathbf{F}$ at the root, which in turn is, at least heuristically, connected with the eigenvalues of the Hessian of the Newton method iterator at the root. Thus, low instability could be connected with the presence of a large basin of attraction for the iterative solver. On the other

hand, again heuristically, under the dynamics of the CGLE the least unstable relative periodic solution would be the one that is easiest for other orbits to approach, and thus low instability would tend to indicate that the solution is in a high traffic area of the attractor, that is, in an area with a large concentration of invariant measure. As noted in § 5.3, observations of the time evolution of typical solutions do reveal their occasional return to a sequence of patterns similar to those manifested by solution 14. This means that the starting values we used for the solver are more likely to be in a neighborhood of solution 14, which would favor convergence to that solution. It is not clear which mechanism, a large basin or an abundance of nearby starting values, is most responsible for the frequency of occurrence of solution 14 among the computed relative periodic solutions.

While solution 14 was the most favored solution, there are other instances of multiple convergence. However, these do not, in general, have the same correlation with the total instability. On one hand, the second most frequently found solution was solution 16, with convergence to it 9 times. This solution does have low instability and is in fact paired with solution 14 in the family described in § 5.3. On the other hand, the next two most frequently found solutions, solutions 3 and 11, had 6 convergences each, but they do not have low instability. In addition, solution 58 has total instability only slightly more than that of solution 14, but the solver found it just once. So while we can, in certain cases, connect the solver behavior to the CGLE dynamics, it is, in general, extremely difficult to understand the behavior of iterative solvers in high dimensions.

6. Discussion and Conclusions. We have described a method of finding relative periodic solutions for differential equations with continuous symmetries and have demonstrated its utility by finding numerous relative periodic solutions for the CGLE, a nonlinear evolution equation with widespread physical and mathematical interest. The various purposes to which periodic orbits are usually put, such as dynamical averaging and control, can be adapted to using relative periodic orbits. In our investigation we found an abundance of relative periodic solutions and an apparent lack of true periodic solutions. This indicates that in the presence of continuous symmetries the use of relative periodic orbits is an attractive option. In addition, the computational burden of finding relative periodic orbits is not significantly higher than that of finding true periodic orbits. It would be of interest to adapt other methods of finding periodic orbits to find relative periodic orbits and systematically compare the various methods.

The most computationally challenging aspect of the numerical procedure is the solution of a system of nonlinear equations for the drift, period, and Fourier coefficients of a relative periodic solution. The use of starting values derived from relative close returns and the choice of solver were critical to our success in identifying solutions. The size of the system considered here, between 2,917 and 3,909 real variables, is at the upper limit of feasible computations at workstation scale. In particular, the solution of linear systems with a (dense) Jacobian as coefficient matrix, which was required as part of the procedure for solving the nonlinear system, could be done using direct methods. For systems with higher dimension than that considered here, one must eventually incorporate the iterative solution of linear systems, along with preconditioning, and the use of parallel computations.

As noted in the introduction, the computation of the relative periodic solutions was undertaken as a first step in understanding of the dynamics of the CGLE with the chosen parameters. This prompts two questions, one specific and the other more gen-

eral. First, is the computed set of relative periodic solutions sufficient to capture the total dynamics in any reasonable sense, and second, is the computation of a collection of relative periodic solutions a good starting point for analyzing and understanding the dynamics of a moderately high-dimensional dynamical system with continuous symmetries?

The general method of analyzing dynamics using a collection of periodic solutions has been investigated in many ways, for many years. A given single periodic orbit will usually not be typical with respect to any globally supported ergodic measure, but under hypotheses that guarantee the existence of a Bowen-Margulis measure (see § 20.1 in [31]), the total collection of periodic orbits yields invariant measures that are equidistributed, and thus the collection of periodic orbits captures the statistics of the system. While these strong hypotheses can never be confirmed in practice, there is a fair amount of empirical evidence that a sufficiently large collection of periodic orbits can capture the global dynamics, but it is usually impossible *a priori* to decide what is "sufficiently large".

The next issue is what part of the dynamics one can hope to capture with a collection of periodic orbits. A typical moderate dimensional chaotic system will display a great deal of dynamical variety, and there is no reason to expect a single, indecomposable attractor. As noted in § 5.5, the method we use is biased towards finding solutions in the closure of the set of typical trajectories. Thus, the appropriate question about the collection of relative periodic solutions is in what sense it predicts the behavior of a typical trajectory.

We have begun this investigation, and the preliminary results are promising. As reported in § 5.4, typical values of the Lyapunov dimension and various functionals were accurately computed using the 77 relative periodic solutions and the weighted averaging scheme proposed in [62]. We have had no success in finding symbolic dynamics, and preliminary attempts to use the sequence of patterns given by the various relative periodic solutions to build up the pattern evolution of a typical trajectory have been unsuccessful. Thus, the question of the predictive value of our collection of relative periodic solutions remains open.

The second question raised above we can answer with an unqualified "yes". Dynamical systems with even moderate dynamical dimension present significant challenges not adequately dealt with using the usual low dimensional theory. The family of relative periodic solutions has allowed us to begin unlocking the intricacies of a flow with Lyapunov dimension of 11.52 (including the flow and symmetry directions). The detailed study of the dynamics of systems with comparable intrinsic dimension is still a rare occurrence in the literature. In this regard we remark that it is common in certain segments of the literature to use the terms "high-dimensional chaos" or "hyperchaotic" for any system with unstable dimension larger than one, and the unstable dimension in our system is typically 5 and varies from 3 to 8 among the relative periodic solutions.

We have found the relative periodic solutions invaluable as a starting point of dynamical analysis for a variety of reasons. First, one can be quite sure of the accuracy of the numerical computations because the solutions can be verified both by integrating the differential equations for a short time interval, $[0, T]$, and by confirming that the drift, period, and Fourier coefficients are solutions of the system of nonlinear algebraic equations. Next, each computed relative periodic solution can be studied in isolation as one piece of the dynamics, as one part of the pattern evolution. Finally, the observations of the individual pieces leads to hypotheses and conjectures

about the whole picture. These can be tested using the collection of relative periodic solutions as a sample space and then the results compared to typical trajectories.

As an illustration of this process we briefly list some of the lines of inquiry that have been opened by our study of the collection of relative periodic solutions. Is there a correlation between spatial aspects of the patterns of a solution and its temporal dynamics, for example, between winding numbers and total instability? How does the unstable dimension variability of the collection of relative periodic solutions contribute to the existence of zero finite-time Lyapunov exponents for the system and other consequences of non-hyperbolicity? What are the global dynamics of our system, for example, how many nontrivial indecomposable attractors are there and how do the invariant fixed symmetry planes fit in with the attractor(s)? What role do the coherent structures or relative equilibria play in the overall *temporal* dynamics of the system; are they contained in the main attractor, or are they isolated and thus dynamically nontypical? Finally, how are the relative periodic solutions and overall dynamics created via bifurcations as R increases from zero to 16?

Nonlinear dynamics has made significant progress in the study of systems with low intrinsic dimension, but the understanding of even moderate dimensional systems still presents significant challenges. We have demonstrated that finding a collection of relative periodic orbits is both computationally feasible and conceptually valuable, and is thus a valuable tool in the important task of understanding moderate dimensional dynamical systems with continuous symmetries.

Appendix A: Properties of Solutions. Table A.1 lists the period T and drift (φ, S) for each of the 77 relative periodic solutions found. The solutions are listed by increasing value of T and have been assigned an identifying number (first column). Also listed is the dimension of the unstable manifold of each solution, along with the largest Lyapunov exponent and total instability (which is given by the sum of the positive Lyapunov exponents).

While most of the relative periodic solutions have trivial $\mathbb{T}^2$-stabilizers, there are a few exceptions. Solutions 3, 15, and 16 have stabilizer $C(1,2)$ (cf. § 3.2), and therefore satisfy $A(x,t) = -A(x+\pi,t)$. Solution 9 has stabilizer $C(1,3)$; it satisfies $A(x,t) = \mathrm{e}^{\mathrm{i}2\pi/3}A(x+2\pi/3,t)$. In addition, solutions 4, 10, and 15 are even about certain points in the spatial domain and solution 15 is odd about certain points in the spatial domain.

Id	T	φ	S	Unstable Dimension	Largest Lyapunov Exponent	Total Instability
1	0.02333	5.36228	3.85441	4	8.85592	28.53243
2	0.05394	2.88491	3.09563	5	5.00321	21.31125
3	0.05394	0.00111	3.97095	5	11.00430	30.30192
4	0.05403	2.93438	3.14159	4	3.57030	9.56834
5	0.05471	4.60939	1.45371	5	6.45679	27.60085
6	0.05561	4.51654	4.70614	5	7.76507	25.39928
7	0.06080	0.24364	2.38876	4	11.31755	36.02733
8	0.08255	4.79599	3.08241	5	10.08510	39.81868
9	0.08748	0.28765	2.44316	6	9.72294	36.31152
10	0.08950	5.02514	3.14159	3	10.72851	27.85965
11	0.10458	2.60234	3.17193	4	5.83393	18.52259
12	0.10797	2.65754	3.12097	3	6.59523	19.55427
13	0.11065	6.05532	0.00321	6	5.10800	19.17581

TABLE A.1
Properties of relative periodic solutions.

Id	T	φ	S	Unstable Dimension	Largest Lyapunov Exponent	Total Instability
14	0.11282	2.60639	3.10577	4	1.88230	5.18967
15	0.11461	2.25004	3.14159	3	6.90750	15.73770
16	0.11492	2.71671	3.14159	5	3.20606	10.12255
17	0.13560	1.82110	2.04598	6	10.56790	42.15027
18	0.13730	0.73763	0.75086	6	13.54288	53.74900
19	0.14037	1.87712	5.73712	7	10.57182	40.07190
20	0.14916	5.81089	1.26773	5	17.19835	50.08455
21	0.15160	1.94728	5.40241	5	6.75385	19.66934
22	0.16098	1.95738	3.85354	5	10.61619	44.38707
23	0.16263	2.56407	5.09938	6	11.43816	35.46420
24	0.16971	5.48891	3.93522	8	7.86379	30.95111
25	0.17500	3.80256	0.98842	6	10.36722	44.23884
26	0.18249	3.40328	6.14235	5	10.19717	36.97288
27	0.18317	3.61256	5.24560	6	12.29563	42.02092
28	0.20146	1.90508	2.41894	6	14.46845	59.36105
29	0.21038	0.70319	1.90349	5	14.85499	60.35458
30	0.21178	5.16441	0.07994	4	5.87695	14.88747
31	0.21766	5.61399	0.00002	5	3.70755	13.08357
32	0.22045	5.15235	0.06622	3	8.28842	16.37539
33	0.22482	4.41470	1.10856	7	13.46647	47.71035
34	0.24430	5.53858	3.60540	6	11.40020	41.36390
35	0.24598	0.88868	4.47924	5	8.78079	35.50550
36	0.24761	2.24375	2.32864	6	15.96544	59.60573
37	0.25234	4.06727	2.73577	5	7.27440	28.49855
38	0.25374	1.47983	2.26736	6	10.89903	43.88382
39	0.26014	5.12178	2.60985	4	5.39730	16.59190
40	0.26623	3.07369	3.27604	6	11.19883	50.85904
41	0.27286	3.69060	3.55692	6	9.88356	37.26567
42	0.27504	2.57465	3.21456	5	5.92789	18.84754
43	0.27679	2.90953	3.10889	4	6.77859	24.98180
44	0.28744	4.84490	1.76031	5	7.34615	23.42338
45	0.28803	2.74448	1.37428	5	8.98143	31.75536
46	0.29746	4.15104	4.09627	6	6.98488	22.53727
47	0.29751	4.32786	1.58049	5	6.18589	20.33417
48	0.30045	4.39783	4.62959	4	5.77264	18.52750
49	0.30392	3.72216	5.49134	6	8.10462	31.10158
50	0.30492	2.74872	3.31013	5	6.89564	21.04823
51	0.30695	4.31730	5.12453	4	9.02700	24.32585
52	0.31343	0.72363	1.98525	5	8.41168	25.64814
53	0.31517	1.87776	1.69240	5	7.79446	24.72635
54	0.31924	5.68308	2.25711	6	11.97732	46.26127
55	0.32350	2.21845	1.26058	5	8.44337	31.00286
56	0.33150	2.42184	3.37971	3	6.90072	15.94646
57	0.33217	4.50138	1.88596	5	6.86741	19.11005
58	0.34035	1.72898	3.15957	3	3.92346	5.99484
59	0.34148	1.74043	3.18504	3	2.56575	6.92418
60	0.34825	6.00790	5.07384	6	10.50662	47.95424
61	0.34892	2.45502	3.11195	4	5.98084	18.44338
62	0.35567	0.76100	0.97929	6	8.70424	25.31565
63	0.36395	1.11216	5.51746	5	4.75266	16.16998
64	0.36621	3.81362	2.39863	6	5.79290	27.12694
65	0.37306	5.25206	1.42035	5	9.96569	30.85402
66	0.37413	1.14509	1.19984	5	8.30154	18.70350
67	0.37619	1.78357	0.93027	5	6.29217	16.68876
68	0.37893	1.44760	0.83458	4	6.92225	20.55719

TABLE A.1
Properties of relative periodic solutions, continued.

Id	T	φ	S	Unstable Dimension	Largest Lyapunov Exponent	Total Instability
69	0.38444	1.83435	1.06175	5	7.33543	20.40029
70	0.38599	1.21873	1.00009	4	7.66270	17.44702
71	0.39128	2.38456	5.34383	4	5.78585	18.67097
72	0.39675	4.79784	3.35390	6	9.55893	30.02312
73	0.40557	3.21458	6.24425	4	6.80844	22.92050
74	0.42108	0.44223	4.10959	4	10.55221	19.44133
75	0.42447	2.27338	3.25431	5	7.58996	26.84563
76	0.44044	3.32603	2.31594	6	7.92846	26.18850
77	0.45840	5.73253	6.25633	5	8.01104	25.60890

TABLE A.1
Properties of relative periodic solutions, continued.

Table A.2 lists properties of the solution $A(x,t) = 0$, which corresponds to Id=0, the plane waves $A(x,t) = \hat{a}_{p,\pm 1} \mathrm{e}^{\pm \mathrm{i}\omega t} e^{\mathrm{i}px}$, which correspond to the identifying numbers 1–4, and the two single-frequency solutions $A(x,t) = B(x)\mathrm{e}^{-\mathrm{i}\omega t}$ (Id=5,6) that were computed numerically. Solution 6 has stabilizer $C(1,2)$ and is even and odd about about certain points in the spatial domain. Solution 5 is even about certain points in the spatial domain.

Id	T	ω	Unstable Dimension	Largest Lyapunov Exponent	Total Instability
0	–	–	14	16.0000	168.0000
1	0.07854	80.0000	8	54.7935	320.2662
2	0.09240	68.0000	8	51.7819	298.3522
3	0.19635	32.0000	8	41.2843	220.1846
4	0.22440	28.0000	8	26.0693	124.4494
5	0.12517	50.1968	10	15.8062	109.0126
6	0.12609	49.8320	7	15.0947	61.4864

TABLE A.2
Properties of solution $A(x,t) = 0$ (Id=0), plane waves $A(x,t) = \hat{a}_{p,\pm 1} \mathrm{e}^{\pm \mathrm{i}\omega t} e^{\mathrm{i}px}$ (Id=1,2,3,4 correspond to p=0,1,2,3, respectively), and single-frequency solutions $A(x,t) = B(x)\mathrm{e}^{-\mathrm{i}\omega t}$ (Id=5,6).

Acknowledgements. V. López thanks O. Stoyanov for helpful discussions and suggestions on preliminary versions of the paper and the CSE program at the University of Illinois for providing excellent computing facilities. The authors thank one of the reviewers for providing references [17, 18].

REFERENCES

[1] Igor S. Aranson and Lorenz Kramer. The world of the complex Ginzburg-Landau equation. *Rev. Mod. Phys.*, 74:99–143, 2002.
[2] Philip J. Aston and Michael Dellnitz. Symmetry breaking bifurcations of chaotic attractors. *Internat. J. Bifur. Chaos Appl. Sci. Engrg.*, 5(6):1643–1676, 1995.
[3] Philip J. Aston and Carlo R. Laing. Symmetry and chaos in the complex Ginzburg-Landau equation. I. Reflectional symmetries. *Dynam. Stability Systems*, 14:233–253, 1999.
[4] Philip J. Aston and Carlo R. Laing. Symmetry and chaos in the complex Ginzburg-Landau equation. II. Translational symmetries. *Physica D*, 135:79–97, 2000.
[5] Michele Bartuccelli, Peter Constantin, Charles R. Doering, John D. Gibbon, and Magnus Gisselfält. On the possibility of soft and hard turbulence in the complex Ginzburg-Landau equation. *Phys. D*, 44(3):421–444, 1990.
[6] P. Boyland. Remarks on the computation of relative periodic solutions. In preparation.

[7] Lutz Brusch, Alessandro Torcini, Martin van Hecke, Martín G. Zimmermann, and Markus Bär. Modulated amplitude waves and defect formation in the one-dimensional complex Ginzburg-Landau equation. *Physica D*, 160:127–148, 2001.

[8] Claudio Canuto, M. Yousuff Hussaini, Alfio Quarteroni, and Thomas A. Zang. *Spectral Methods in Fluid Dynamics*. Springer-Verlag, 1988.

[9] H. Chaté. Disordered regimes of the one-dimensional complex Ginzburg-Landau equation. In *Spatiotemporal Patterns in Nonequilibrium Complex Systems*, volume 21 of *Sante Fe Institute Studies in the Sciences of Complexity*, pages 33–50. Addison-Wesley, 1994.

[10] Won Gyu Choe and J. Guckenheimer. Computing periodic orbits with high accuracy. *Comput. Methods Appl. Mech. Engrg.*, 170:331–341, 1999.

[11] F. Christiansen, P. Cvitanović, and V. Putkaradze. Spatiotemporal chaos in terms of unstable recurrent patterns. *Nonlinearity*, 10:55–70, 1997.

[12] Peter Constantin. A construction of inertial manifolds. In *The Connection Between Infinite-Dimensional and Finite-Dimensional Dynamical Systems (Boulder, CO, 1987)*, volume 99 of *Contemp. Math.*, pages 27–62. Amer. Math. Soc., Providence, RI, 1989.

[13] P. Cvitanović, R. Artuso, R. Mainieri, G. Tanner, and G. Vattay. *Chaos: Classical and Quantum*. Niels Bohr Institute, Copenhagen, 2003. `www.nbi.dk/ChaosBook`.

[14] Predrag Cvitanović. Chaotic field theory: A sketch. *Physica A*, 288:61–80, 2000.

[15] H. Dang-Vu and C. Delcarte. Spatial heteroclinic bifurcations of time periodic solutions to the Ginzburg-Landau equation. *Quart. Appl. Math.*, 57:459–472, 2000.

[16] J. E. Dennis, Jr. and Robert B. Schnabel. *Numerical Methods for Unconstrained Optimization and Nonlinear Equations*. SIAM, 1996. (Reprint of 1983 edition).

[17] C. P. Dettmann and P. Dahlqvist. Computing the diffusion coefficient for intermittent maps: Resummation of stability ordered cycle expansions. *Phys. Rev. E*, 57:5303–5310, 1998.

[18] C. P. Dettmann and G. P. Morriss. Stability ordering of cycle expansions. *Phys. Rev. Lett.*, 78:4201–4204, 1997.

[19] E.J. Doedel, A.R. Champneys, T.F. Fairgrieve, Yu.A. Kuznetsov, B. Sandstede, and X. Wang. AUTO97: Continuation and bifurcation software for ordinary differential equations (with HomCont). Technical report, Concordia University, 1997. `http://indy.cs.concordia.ca/auto/`.

[20] Arjen Doelman. Slow time-periodic solutions of the Ginzburg-Landau equation. *Physica D*, 40:156–172, 1989.

[21] Arjen Doelman and Edriss S. Titi. Regularity of solutions and the convergence of the Galerkin method in the Ginzburg-Landau equation. *Numer. Funct. Anal. Optim.*, 14(3-4):299–321, 1993.

[22] Charles R. Doering, John D. Gibbon, Darryl D. Holm, and Basil Nicolaenko. Low-dimensional behaviour in the complex Ginzburg-Landau equation. *Nonlinearity*, 1:279–309, 1988.

[23] M. J. Field. Equivariant dynamical systems. *Trans. Amer. Math. Soc.*, 259(1):185–205, 1980.

[24] M. J. Field. Equivariant dynamics. In *Multiparameter Bifurcation Theory (Arcata, Calif., 1985)*, volume 56 of *Contemp. Math.*, pages 69–96. Amer. Math. Soc., Providence, RI, 1986.

[25] M. Frigo and S. G. Johnson. FFTW: An adaptive software architecture for the FFT. In *ICASSP Conference Proceedings*, volume 3, pages 1381–1384, 1998. `http://www.fftw.org/`.

[26] J.-M. Ghidaglia and B. Héron. Dimension of the attractors associated to the Ginzburg-Landau partial differential equation. *Phys. D*, 28(3):282–304, 1987.

[27] Martin Golubitsky, Ian Stewart, and David A. Schaeffer. *Singularities and Groups in Bifurcation Theory. Volume II*. Springer-Verlag, 1988.

[28] John Guckenheimer and Brian Meloon. Computing periodic orbits and their bifurcations with automatic differentiation. *SIAM J. Sci. Comput.*, 22:951–985, 2000.

[29] M. S. Jolly, R. Temam, and C. Xiong. Convergence of a chaotic attractor with increased spatial resolution of the Ginzburg-Landau equation. *Chaos Solitons Fractals*, 5(10):1833–1845, 1995.

[30] Todd Kapitula and Stanislaus Maier-Paape. Spatial dynamics of time-periodic solutions for the Ginzburg-Landau equation. *Zeitschrift für Angewandte Mathematik und Physik*, 47:265–305, 1996.

[31] Anatole Katok and Boris Hasselblatt. *Introduction to the Modern Theory of Dynamical Systems*, volume 54 of *Encyclopedia of Mathematics and its Applications*. Cambridge University Press, Cambridge, 1995.

[32] Laurence R. Keefe. Dynamics of perturbed wavetrain solutions to the Ginzburg-Landau equation. *Stud. Appl. Math.*, 73(2):91–153, 1985.

[33] Eric J. Kostelich, Ittai Kan, Celso Grebogi, Edward Ott, and James A. Yorke. Unstable dimension variability: A source of nonhyperbolicity in chaotic systems. *Phys. D*, 109(1-

2):81–90, 1997.
[34] Martin Krupa. Bifurcations of relative equilibria. *SIAM J. Math. Anal.*, 21(6):1453–1486, 1990.
[35] Jeroen S. W. Lamb and Claudia Wulff. Reversible relative periodic orbits. *J. Differential Equations*, 178(1):60–100, 2002.
[36] Yueheng Lan and Predrag Cvitanović. Variational method for finding periodic orbits in a general flow. *Phys. Rev. E*, 69:016217, 2004. `arXiv:nlin.CD/0308008`.
[37] S. L. Lau, Y. K. Cheung, and S. Y. Wu. A variable parameter incrementation method for dynamic instability of linear and nonlinear elastic systems. *Journal of Applied Mechanics*, 49:849–853, 1982.
[38] Kenneth Levenberg. A method for the solution of certain non-linear problems in least squares. *Quart. Appl. Math.*, 2:164–168, 1963.
[39] C. David Levermore and Marcel Oliver. The complex Ginzburg-Landau equation as a model problem. In *Dynamical Systems and Probabilistic Methods in Partial Differential Equations*, volume 31 of *Lectures in Appl. Math.*, pages 141–190. Amer. Math. Soc., Providence, RI, 1996.
[40] F. H. Ling and X. X. Wu. Fast Galerkin method and its application to determine periodic solutions of non-linear oscillators. *Internat. J. Non-Linear Mech.*, 22:89–98, 1987.
[41] Paul Manneville. Liapunov exponents for the Kuramoto-Sivashinksy model. In *Macroscopic Modelling of Turbulent Flows*, U. Frisch *et al.*, eds., Lecture Notes in Physics 230, pages 319–326. Springer-Verlag, 1985.
[42] Donald W. Marquardt. An algorithm for least-squares estimation of nonlinear parameters. *J. Soc. Indust. Appl. Math.*, 11:431–441, 1963.
[43] Jerrold E. Marsden and Tudor S. Ratiu. *Introduction to Mechanics and Symmetry*, volume 17 of *Texts in Applied Mathematics*. Springer-Verlag, New York, second edition, 1999.
[44] A. Mielke. The Ginzburg-Landau equation in its role as a modulation equation. In *Handbook of Dynamical Systems, Vol. 2*, B. Fiedler, ed., pages 759–834. Elsevier Science, 2002.
[45] Willard Miller, Jr. *Symmetry Groups and Their Applications*. Academic Press, Inc., 1972.
[46] H. T. Moon, P. Huerre, and L. G. Redekopp. Transitions to chaos in the Ginzburg-Landau equation. *Phys. D*, 7(1-3):135–150, 1983.
[47] J. J. Moré, B. S. Garbow, and K. E. Hillstrom. User guide for `minpack-1`. Technical Report ANL-80-74, Argonne National Laboratory, Argonne, IL, 1980. `http://www.netlib.org/minpack/`.
[48] Jorge J. Moré. The Levenberg-Marquardt algorithm: Implementation and theory. In *Numerical Analysis*, G. A. Watson, ed., Lecture Notes in Math. 630, pages 105–116. Springer-Verlag, 1977.
[49] Peter J. Olver. *Equivalence, Invariants, and Symmetry*. Cambridge University Press, 1995.
[50] Edward Ott. *Chaos in Dynamical Systems*. Cambridge University Press, 2002.
[51] M. J. D. Powell. A hybrid method for nonlinear equations. In *Numerical Methods for Nonlinear Algebraic Equations*, P. Rabinowitz, ed., pages 87–114. Gordon and Breach, London, 1970.
[52] Keith Promislow. Time analyticity and Gevrey regularity for solutions of a class of dissipative partial differential equations. *Nonlinear Anal.*, 16(11):959–980, 1991.
[53] Keith Promislow and Roger Temam. Localization and approximation of attractors for the Ginzburg-Landau equation. *J. Dynam. Differential Equations*, 3(4):491–514, 1991.
[54] Timothy D. Sauer. Shadowing breakdown and large errors in dynamical simulations of physical systems. *Phys. Rev. E (3)*, 65(3):036220, 5, 2002.
[55] Peter Takáč. Bifurcations to invariant 2-tori for the complex Ginzburg-Landau equation. *Appl. Math. Comput.*, 89:241–257, 1998.
[56] Roger Temam. *Infinite-dimensional Dynamical Systems in Mechanics and Physics*, volume 68 of *Applied Mathematical Sciences*. Springer-Verlag, New York, 1997.
[57] Minoru Urabe and Allen Reifer. Numerical computation of nonlinear forced oscillations by Galerkin's procedure. *J. Math. Anal. Appl.*, 14:107–140, 1966.
[58] Martin van Hecke. Coherent and incoherent structures in systems described by the 1D CGLE: Experiments and identification. *Physica D*, 174:134–151, 2003.
[59] W. van Saarloos. The complex Ginzburg-Landau equation for beginners. In *Spatiotemporal Patterns in Nonequilibrium Complex Systems*, volume 21 of *Sante Fe Institute Studies in the Sciences of Complexity*, pages 19–31. Addison-Wesley, 1994.
[60] Claudia Wulff, Jeroen Lamb, and Ian Melbourne. Bifurcation from relative periodic solutions. *Ergodic Theory Dynam. Systems*, 21(2):605–635, 2001.
[61] Claudia Wulff and Mark Roberts. Hamiltonian systems near relative periodic orbits. *SIAM J. Appl. Dyn. Syst.*, 1(1):1–43, 2002.
[62] Scott M. Zoldi and Henry S. Greenside. Spatially localized unstable periodic orbits of a high-dimensional chaotic system. *Phys. Rev. E*, 57:R2511–R2514, 1998.